1.1 Literature survey

Most of chemical researches begin with answering questions related to molecular structure owing to the great connection between structure with properties and functions. This becomes particularly exciting when new molecules with novel structures are synthesized or identified if there is the prospect for novel physical or chemical properties, as might be suggested from known correlations.

Although the determination of molecular structure has long essentially been depending upon spectroscopic tools, however, another set of tools has emerged in the last few decades. It is the direct application of rigorous quantum mechanical principles by way of large scale computations or the application of calculational methods devised from fundamental chemical and physical concepts [1].

One of the first steps in most theoretical approaches to the electronic structure of molecules is the use of orbital models. Typically, an orbital model such as Hartree Fock SCF theory provides an excellent starting point which account for the bulk " ≈99%" of the total energy of the molecule, which was performed by **W.J. Hehre, et.al.,**[2].

We represent here, some of the abstracts that are related to the topics treated in this thesis:

C.D. Sherrill and H.F. Schaefer, [3] investigated a number of configuration interaction (CI) wave functions which incorporate the dominant effects of triple and quadrable substitutions. Natural orbitals were employed from a configuration interaction including single and double excitation (CISD)

procedure, then the orbitals were partitioned into subspaces of varying importance, and electron configurations were classified according to how they occupied each of the subspaces.

A.D. Becke, [4] reported a gradient-corrected exchange-energy functional with the proper asymptotic limit. Current gradient-corrected density-functional approximations for the exchange energies of atomic and molecular systems failed to reproduce the correct 1/r asymptotic behavior of the exchange-energy density. This functional, containing only one parameter, fits the exact Hartree-Fock exchange energies of a wide variety of atomic systems with remarkable accuracy, surpassing the performance of previous functionals containing two parameters or more.

A. Glasner and F.C. Tompkins, [5] noted the various relationships which exist between the absorption band maxima of colored alkali metal halides and proposed some simple empirical rules for calculating certain crystal parameters from the position of these maxima.

D.E. Parry, [6] described a method for the rapid evaluation of the electrostatic potential near the surface of an ionic crystal. The deviation of the potential from its behavior in the crystal bulk was discussed with reference to X-ray photoelectron spectroscopy. Application of the method included crystal faces where redistribution of charge and lattice reconstruction occurs near the surface. The {100}, {110} and {111} faces of the unreconstructed ionic NaCl crystal were studied.

W. Gellermann, [7] applied the color centers in alkali halide crystals as high-gain active materials in tunable solid state lasers. Using various color center types and host lattices, the combined tuning range of color center lasers covers

presently the near-infrared region from about 0.8 to 4 μm. Studied the optical properties of the main laser-active color center types, the techniques used for their production, and their laser characteristics. Furthermore, a brief summary was given on the application of color center lasers.

A.S. Shalabi, et.al., [8] examined the bulk and surface properties of exciton bands near F^+, F and F^- centers (α, β and γ bands), diffusion of electron centers (F^+, F and F^-) and adsorptivity of atomic H over the undefected and defected (F^+, F and F^-) surfaces of LiH using an ab initio embedded cluster method at the Hartree-Fock approximation and Moller-Plesset second-order perturbation correction. The results confirm the exclusive dependence of the exciton bands on the type of the electron center. The activation energy for bulk diffusion increases monotonically in the series $F^+ \rightarrow F \rightarrow F^-$. Bulk and surface relaxation effects are more important for F^+ than for F and F^- centers. The introduction of F or F^-center changes the nature of adsorption from physisorption to chemisorption. The introduction of F^-center changes the nature of LiH surface from an insulating surface to a semiconducting surface. As F and F^- centers are introduced, the HOMO and LUMO levels of the substrate shift to a higher energy and the band gaps become narrower. These changes in the electronic structure make charge transfer between adsorbate and substrate energy levels and spin pairing with F center more facile in the course of adsorbate-substrate interactions.

A.S. Shalabi, et.al., [9] made an attempt to apply the Glasner-Tompkins relation to LiH and LiF crystals and to examine the reorientation of H and H_2 interstitials in LiF crystal using the matrix Hartree-Fock method of ab inito theory.

A finite lattice, in which the Coulomb potential in the central region closely approximates the Madelung potential in the unit cell of the host crystal, is constructed. The results emphasize the strong dependence of the difference between the exciton band and the F^- center band on the halide species and suggest a mechanism by which the U band bleaches in LiF crystal. The energetically preferred orientation of H_2 interstitials in the <110> plane supports the conclusion that the mobile H_2 molecules, while being unable to react with isolated *F* centers, can react with *F* center pairs (*M* centers) to produce the complex *U* centers.

A.S. Shalabi, et.al., [10] constructed a finite LiH lattice whose Madelung potential in the central region closely approximates the Madelung potential in the host crystal. Hartree-Fock calculations were then carried out on lithium hydride clusters both within the crystal and as isolated species. The many body expansion terms and the probability of ionic motions, which result in diffusion, were examined and relaxation around diffused ions was taken into account. Calculations confirm that the many body expansion terms in the crystal environment were both convergent and smaller than for the isolated clusters. The two-ion rotation mechanism is the most probable. The barrier height for cation diffusion is less than for anion diffusion suggesting easier transfer of cations rather than anions within the LiH crystal. The results were correlated with those reported previously on LiF crystal.

F. Finocchi, et.al., [11] studied the oxygen deficient MgO (100) surfaces by means of total energy calculations, within the density functional theory. Selected surface configurations presenting increasing densities of neutral oxygen vacancies, ranging from 12.5% to 100%, are considered. Showing that the electronic structure is characterized by occupied states in the gap which result

either from the hybridization of atomiclike orbitals localized on vacancy sites, or involve surface magnesium orbitals. The formation energy of oxygen vacancies is calculated as a function of the vacancy concentration.

G.C. Benson, et.al., [12] extended previous calculations of the distortion in the outermost layer at a {100} face of an alkali halide hemicrystal with NaCl type structure to considered deformations occurring within the first n layers. The model permits the ions of the surface region to relax in a direction normal to the face and the equilibrium configuration is determined by minimizing the energy of the system.

G.P. Summers, et.al., [13] reported experimental measurements and theoretical calculations which may resolve some of the remaining difficulties associated with photoemission from anion vacancies in thermochemically reduced MgO crystals. The intensities of the 2.3 and 3.2 eV luminescence bands are found to be strongly influenced by both the concentrations of H^- ions and anion vacancies, and also by the intensity of the ~ 5.0 eV exciting light.

U. Landman, et.al., [14] applied the quantum path-integral molecular-dynamics method to explore the structure, energetics, and dynamics of an excess electron interacting with an alkali halide cluster. Four distinct modes of electron localization were established, which depend on the cluster composition, size, and structure; they involve an internal *F* center defect, an external surface state, dissociative detachment of an alkali atom, and structural isomerization induced by electron attachment.

S. Choi and T. Takeucili, [15] showed that the *F*-type color centers in oxide crystals were qualitatively different from the color centers of alkali halides. A semi-quantitative discussion was followed by the results of an Xα self-

consistent-field calculation for the α-$A_{12}O_3$ crystal. An oxygen-ion vacancy in α-alumina is a deep electron trap, the ground state of which lies between the two valence bands, unlike the *F* center of alkali halides whose ground state lies between the valence and conduction bands. The two electrons in the trap are stabilized by a hole.

T. Kojima, [16] presented theoretical investigation of the electronic states of the *F*-center in LiF by taking into account the detailed atomic structure of the crystal. The Hamiltonian of an *F*-center including polarization effects was presented. The polarizabilities of the ions in the crystal were determined from the static and high frequency dielectric constants. Approximate eigenfunctions and energy levels were calculated with the use of variational wave functions comprising linear combinations of the 2s and 2p atomic functions on the six lithium ions adjacent to the missing negative-ion site. For both the ground and excited states, the resulting wave functions have larger coefficients of the 2p functions than those of the 2s functions. The first optical excitation energy was obtained to be somewhat smaller than the experimental value; possible sources of this discrepancy were discussed.

J. Wiesenfield, et.al., [17] measured the configurational relaxation time for the $F_A(II)$ center in KCl:Li with use of picosecond laser techniques. The saddle-point configuration of the electronically excited state is stabilized by means of multiphonon emission, and has a zero-temperature lifetime of 13 psec.

E.C. Honea, et.al., [18] reported the measurements of abundances and electronic properties of neutral sodium halide clusters, Na_nX_{n-1} ($n<100$), which demonstrate a remarkable range of excess-electron dominated behavior. Clusters, which can form a cubic lattice containing a single anion vacancy, have the electron localized in the vacancy, stabilizing the cluster against fragmentation.

For the singular values of n, which correspond to a filled cubic lattice, the electron is very weakly bound. A simple quantitative model of electron localization is proposed to account for the observed patterns of abundances and electron binding energies.

P. Xia and L.A. Bloomfield, [19] reported photoelectron spectra of sodium chloride cluster anions, $(NaCl)_nNa^-$ (n=1-21), which contain two excess electrons. Three distinct types of spectra were observed, corresponding to three different modes for accommodating the two electrons. Suggested that, in some clusters, the electrons form spin pairs that either occupy a single anion vacancy as an *F* color center or localize on a Na^+ cation to form a Na^- anion. In other clusters, the two electrons separately occupy a pair of anion vacancies as a double *F* color center.

H. Hakkinen and M. Manninen, [20] studied structure, stability, dynamics, and the electronic structure of small sodium clusters with 2 to 12 atoms adsorbed on the NaCl <001> surface using an ab initio total energy method. The interaction between the ideal surface and the metal cluster has been found to be weak due to a large energy gap between the surface and the cluster single electron states. As a result, the geometry and the electronic structure of the smallest clusters ($N \leq 6$) is distorted only slightly if compared to the free clusters. The cluster binding energy to the surface has a local maximum at N=6. The weak cluster-surface interactions are modified dramatically in the presence of surface *F* centers (missing chlorine atoms). The *F* center increases the adsorption energy of sodium adatom by 1eV and changes the nature of adsorption from physisorption to chemisorption. Similarly, the binding of small sodium clusters to the surface is enhanced by *F* centers.

Y. Chen, et.al., [21] used optical absorption and luminescence experiments to study the photoconversion of neutral oxygen vacancies (*F* centers) in MgO single crystals thermchemically reduced at elevated temperatures. In crystals with an undetectable concentration of hybrid ions and a moderate concentration of *F* centers (1017 cm^{-3}), excitation with UV-light produces positively charged anion vacancies (F^+ centers) and electrons which are subsequently trapped at impurities. Under continuous excitation, the F^+ centers release holes, which are trapped at cation vacancies charge compensated by impurities.

R.I. Eglitis, et.al., [22] studied the self-consistent atomic and electronic structure of the two basic electron defects in MgO crystals- F^+ and *F* centers (one and two electrons trapped by an O vacancy) by using semi-empirical quantum chemical simulations of 125-atom clusters. The calculated absorption and luminescence energies agree with the experimental data, the excited states of both defects were found to be essentially delocalized over nearest-neighbor cations. The mechanism of the $F^+ \rightarrow F$ photoconversion was discussed.

F. Bassani and N. Inchaupe, [23] determined the positions of the α band and the β band relative to the first maximum of the fundamental absorption bands by using the traditional model of the exciton. The β band is considered to be due to an exciton created in immediate vicinity of an *F* center and α band to an exciton created in the immediate vicinity of a negative-ion vacancy. Simple assumptions were made in performing the calculations of the energy required to create the exciton. The results obtained agree satisactorily with the available experiments.

A.Y. Kung, et.al., [24] reported the Unrestricted-Hartree-Fock cluster calculations, which include the nearest-neighbor ions of *F* centers in the lithium and potassium halides, and of F_A(Li) centers in the potassium halides. The Coulomb potential of a surrounding lattice of point ions was included. Optical-absorption energies, including F_A splitting, were found to be in satisfactory agreement with experimental.

J.A. Mejias, [25] studied the adsorption of noble metal atoms (Cu, Ag, and Au) on the NaCl (l00) surface by using an embedded cluster approach. Different models for the surface were used in order to study the convergence of the properties participating in the bonding. The use of a suitable embedding and the lack of participation of the sodium 3s orbitals allowed for reliable results with small clusters. Adsorption energies and metal-surface distances were calculated by using ab initio Hartree-Fock calculations and including the correlation energy at the second order of perturbation theory. An effective core potential approximation, which includes relativistic mass-velocity corrections for silver and gold, was used for the inner electrons of the metal. Corrections for the basis set superposition error were considered as well. The interaction energy was small (≈ 0.l eV) and the distances long (>3 Å) for all models considered. Adsorption has no noticeable chemical contributions. This was explained by resorting to the electronic structure of metal and surface. Most of the binding energy was due to electrostatic and dispersion forces.

J.F. Hamilton, [26] studied the light sensitive elements of conventional photographic materials that are crystallites principally of the bromide or chloride salts of silver. Certain chemical modifications employing sulphur and gold compounds are used to maximize the response, and organic dyes are adsorbed to provide sensitivity throughout the visible spectrum. Absorption of a few photons results in the reductive formation of one or more clusters of silver or gold atoms

on the surface. These clusters act as catalysts to promote further reduction of the host crystallites during photographic development. The success of the system depends upon the particular physical properties of the silver halides, such as their bonding and electron structure, the dielectric properties, the point defect structure, and the electronic transport characteristics. A nucleation and growth mechanism operates to provide several of the favorable features of the process, and the chemical treatments used to optimize the competition between these desirable steps and the unwanted recombination of electronic carriers.

P. Fayet, et.al., [27] observed the development after exposure to beams containing Ag4+ or larger aggregates (Ag_5^+, Ag_7^+, Ag_9^+). No development occurred after exposure to beams of smaller cluster sizes (Ag_1^+, Ag_3^+). These experiments prove directly the existence of a "critical" size required for catalyzing development. This size may depend on the development conditions (e.g., the redox potential), as suggested by theories.

C.R. Baetzold, [28] examined nuclei of Cd, Ag and Pd that containing up to thirty atoms by using extended Hückel and CNDO molecular orbital calculations. These particles represent latent image and as such, their electronic properties are important in determining catalytic properties involved in development. The nuclei were isolated or in the presence of substrate, such as AgBr or graphite. Bonds are formed in this treatment by overlap of atomic wavefunctions and the molecular orbitals that result indicates electron delocalization throughout the system. Isolated particles of this size have calculated cohesive energy roughly 1/3 of bulk experimental values reflecting the high surface/volume ratio. The most stable geometric form of small particles is linear for Ag and Cd and symmetric three-dimensional for Pd. When placed on substrates, other geometries become more stable. Electron affinity is an increasing function of Ag particle size, indicating better electron-accepting

properties of the larger particles. Silver atoms on a silver halide or graphite substrate donate electrons to the substrate. One silver atom on AgBr acquires a positive charge equal to a lattice cation. As the size of silver particle increases, the average charge on the particle decreases, indicating an increase in stability. The electron affinity of Ag particles on AgBr indicates ability increasing with size to accept electrons from the conduction band.

C.R. Baetzold, [29] applied extended Hückel and CNDO molecular orbital calculations to silver clusters adsorbed on various surface sites of AgBr. Positive kink sites possess sufficient activity to promote electron trapping and silver-atom aggregation whereas other sites were much less effective. Two-atom Ag clusters compete with positive kink sites for photoelectrons, since each has nearly the same electron affinity.

1.2 Color center lasers

The first observation of laser action with color centers as active material was reported in 1965 by Fritz and Menke [30]. All color center lasers realized so far are based on electronic defects, that is electrons bound to acombination of anion vacancies (intrinsic defects), or electrons bound to acombination of anion vacancies and adjacent impurity ions (extrinsic defects). The simplest electronic defect is the *F* center (from the German word Farbe meaning color) consisting of an electron bound to the net positive charge of an anion vacancy, thus forming localized electronic states with hydrogen-like character in the forbidden energy gap. Although *F* center is not laser active itself, it serves as an important building block for the formation of all laser active "*F* aggregate centers". The *F* center will be used as an example to briefly summarized the basic properties of color center [31] which are common to all laser active centers, i.e. structure of the energy level diagram, nature of the optical transitions and their broadening due to electron-phonon coupling.

In Figure (1.1), only the electronic energies are plotted, referenced to the conduction band, while lattice energies are ignored. The lowest energy levels in the ground state ionic configuration (left side of Figure (1.1)) are positioned fairly deep below the conduction band. The fundamental absorption transition energy 1s $\rightarrow$2p is in good agreement with the experimentally observed value (2.7eV or 450 nm).

The close proximity of the relaxed excited state RES of the *F* center to the conduction band edge has an important consequence for the formation of other defects. Since the separation is only about 0.1eV, *F* center electrons can be easily thermally excited from the RES into the conduction band at 200-270K crystal temperature depending on the particular host crystal. The empty anion

vacancies left behind can migrate by thermally-activated diffusion and participate in the formation of more complex *F* aggregate centers.

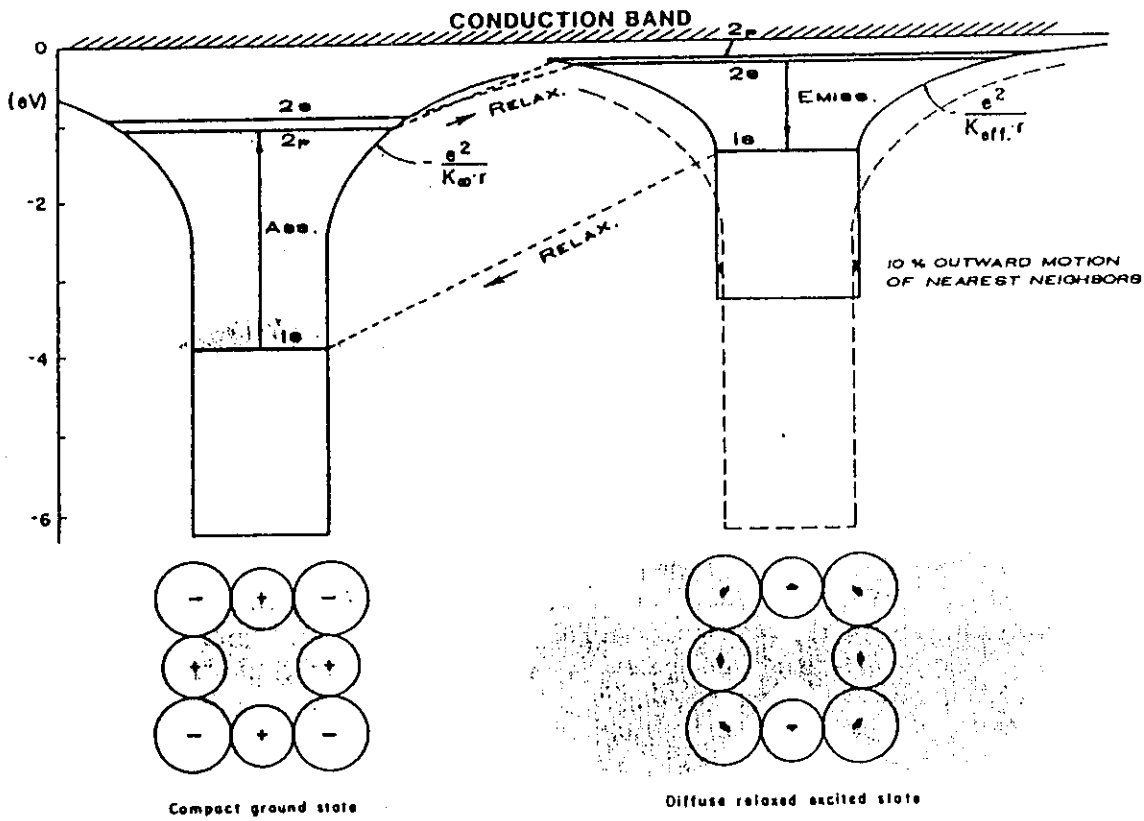

Figure (1.1): Binding potentials and energy levels of the *F* center electron, shown on the left side for the ground state configuration, and on the right side for the relaxed excited state configuration.

The production of color centers in crystals generally depends on thermal or radiation treatments. One major problem with color centers lasers is the lack of stability of color centers at room tempreture. The mobility of electrons and ions in the host crystals can cause the number of color centers to decay with time or change into aggragate centers.

The possible energy level structure of a color center electron is critically influenced by the instantaneous shape and depth of the electronic binding potential. This potential is determined mainly by the distance and geometrical arrangement of the nearest surrounding lattice ions, which oscillate around their equilibrium positions. On the other hand, the ionic equilibrium positions of the surrounding ions are determined by the average electronic charge distribution. The ionic equilibrium is thus different for different electronic states.

The electron phonon coupling and its effect on the optical transitions can be illustrated with the well known configuration coordinate (CC) diagram [32] illustrated in Figure (1.2) for the case of strong coupling (upper part) and weak coupling (lower part). In the CC diagram the electronic energies in ground and excited state are plotted vs the displacement of usually a single configuration coordinate Q. Within the harmonic approximation the electronic states are parabolas. The strength of the electron phonon coupling is reflected by the different equilibrium positions of the parabolas. For strong coupling the shift is large and for weak coupling it is small.

Starting from the ground state, an optical excitation of the color center produces a transition into the excited state at fixed nuclear coordinates (Franck-Condon principle). Due to the Gaussian-shaped probability function for the lowest vibrational state the transition starts with the highest probability from the equilibrium position Q_1. The electronic distribution reached after excitation in the excited state is not in equilibrium with the lattice at Q_1. As a consequence the ions oscillate towards new equilibrium positions. The time needed for this relaxation is in the sub-picosecond range [33]. The electron-lattice system will reach the new equilibrium position Q_2, the RES. After the mean lifetime, the excited electron returns in a vertical emission process back to the ground state, and a subsequent lattice relaxation completes the optical cycle.

For tunable laser applications the electron-phonon coupling provides the following important properties of color centers:

(1) It produces homogeneously (phonon) broadened and Stokes-shifted optical transition bands.

(2) Since the relaxation times are in the sub-picosecond range and are therefore several orders of magnitude smaller than the RES lifetime, an almost ideal four energy level scheme exists, in which each center excitation leads to a population inversion between the luminescence levels.

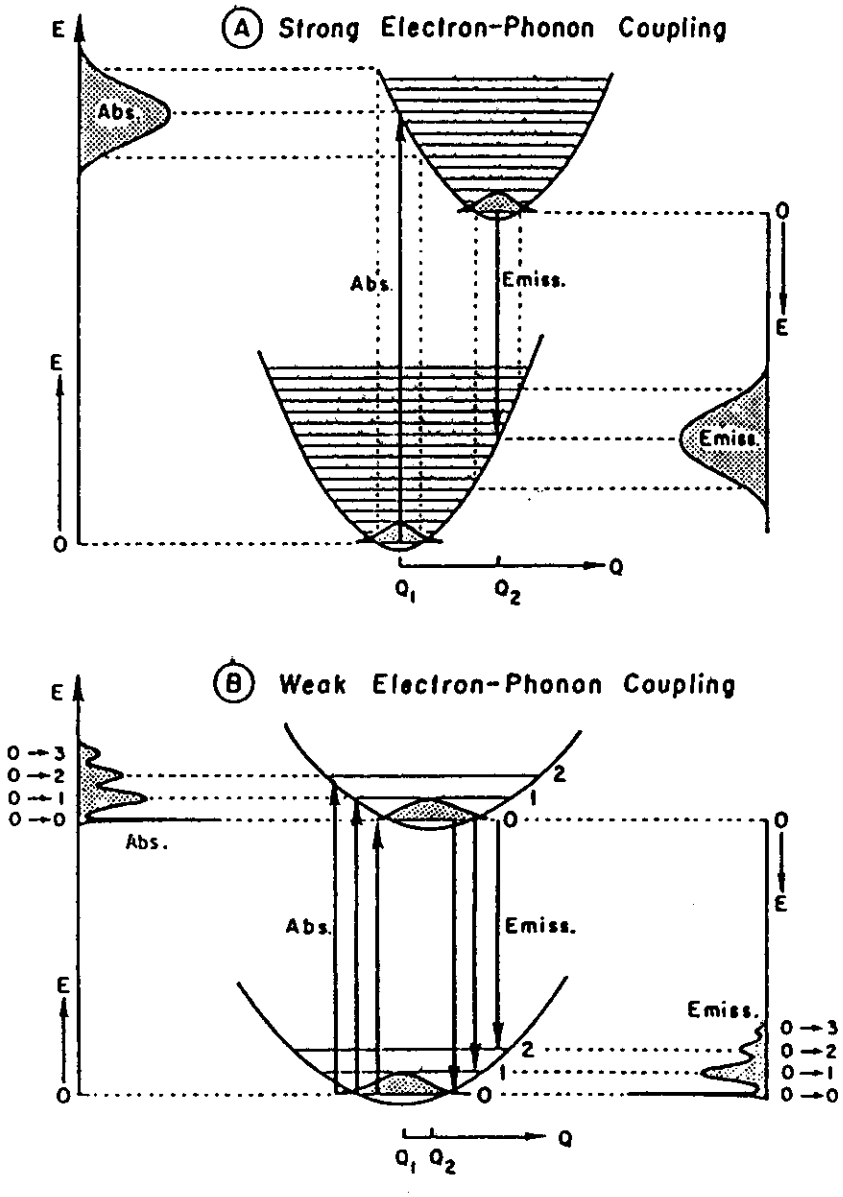

Figure (1.2): Configuration coordinate diagrams for color centers with strong (A) and weak electron-phonon coupling (B), with illustration of band shapes of optical transitions.

1.2.1 The structure of color centers in the alkali halides

Alkali halides are ionic crystals having a large forbidden energy gap between valence and conduction bands (~ 8 eV for KCl). Pure crystals are optically transparent over a corresponding wide spectral range limited in the ultraviolet by electronic excitation of the halide ions and in the infrared by excitation of lattice vibrations. Melting points of the crystals are below 1000°C and thus still in a convenient temperature range for crystal growth. Large single crystals are easily grown from alkali halide powders, with high chemical purity and also high optical quality.

The most important physical property of any material considered for tunable laser applications is the existence of strong and broad optical transitions. Color centers in alkali halides fulfil this requirement particularly well. In general, electrons associated with the defect interact strongly with the surrounding vibrating crystal ions, resulting in optical transitions, which are allowed in a broad band around a defect specific central transition wavelength. Due to the large variety of available defect types and host lattices, optical transitions can be found which cover a wide and important wavelength rang from ~ 0.3 to 4μm.

In the alkali halides, the band gap between the valence and conduction levels is typically 9 to 10 eV. Photons of appropriate energy liberate electrons from the halide ions, simultaneously producing positive holes or simply holes. This process corresponds to an electron being removed from the valence band into the conduction band. Less energetic photons do not ionize the anions but instead excite them into higher excited states. These excitations involve transitions of the valence electrons to exciton states, which produce absorption bands near the fundamental absorption edge of the crystal. The exciton is

envisaged as a mobile, uncharged particle consisting of an electron in an excited state bound to a positive hole. As indicated schematically in Figure (1.3), the exciton states lie just below the conduction band.

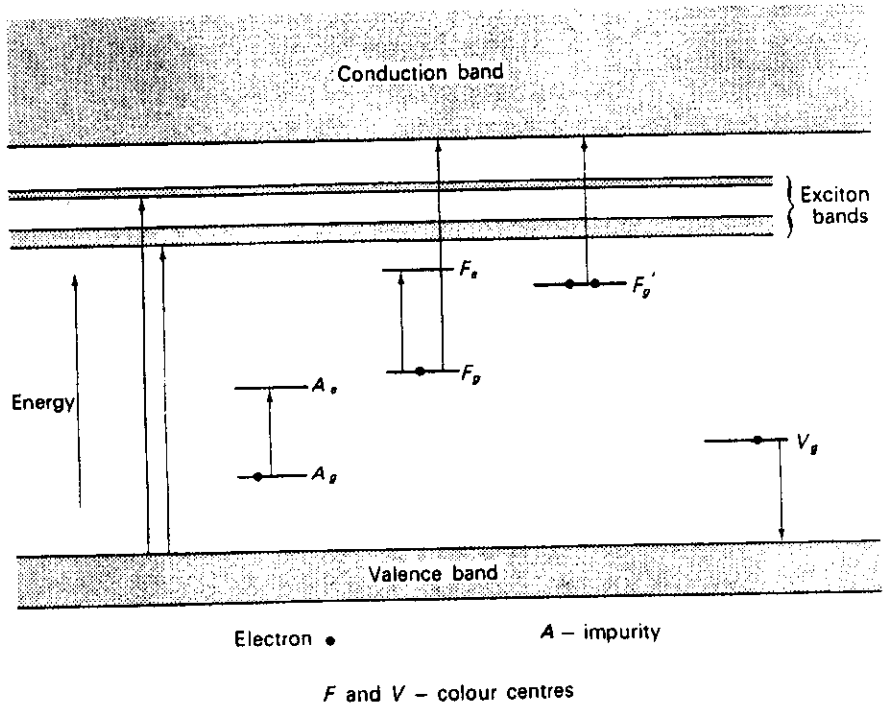

Figure (1.3): Schematic representation of the band structure of an alkali halide crystal, showing transitions associated with the presence of defect levels in the band gap. The subscripts refer to ground (g) and exited (e) states [34].

In order to explain the emission properties of the *F* center, in particular the anomalously long lifetime (~ 1 μs in NaCl), Fowler [31] assumed that after optical excitation the next-nearest neighboring ions of the vacancy relax outwards by ~ 10% of their ground state distance (in keeping with the well-known Franck-Condon model). The calculation then results in a strong decrease of the potential well depth and a corresponding shift of the electronic states to higher energies. The total energy of the system (conduction electron plus vacancy) will decrease as the lattice around the vacancy relaxes and phonons are released. So the

relaxed excited state (RES) will actually be positioned below the state reached in absorption.

1.2.1.1 Defect production mechanisms

Exposure of alkali halides to ionizing radiation produces in general a large variety of defects. Their individual stability is critically influenced by the purity of the crystal, the temperature, the radiation dose, and the conditions for thermally induced reactions. In the last few decades a vast amount of background information has accumulated on the detection and identification of most of these radiation induced defects. The most basic problem, to identify and explain the elementary process of defect formation by ionizing radiation at low temperatures in pure crystals, has been investigated in most detail [35,36].

The presence of impurities can change both the relative concentrations of the defects formed under ionizing radiation and their thermal stabilities. An example is doping with Tl^+ or Ag^+ impurity [37]. Under electron irradiation at low temperatures these ions act as strong electron traps.

Exposure of the radiated crystal to light leads to an excitation of defect electrons. If their final state lies in the conduction band, a transfer of the electron to other defects with electron trapping properties is possible. This causes an ionization of the original defect, which then might become mobile and react with other centers. If the excitation leads to higher bound states, radiationless de-excitations may occur which involve center reorientations and when repeated induce a migration of the center through the lattice.

For the production of F_2^+ centers, electron irradiation of the crystals at temperatures below the anion vacancy mobility range produces essentially only

the atomic defects, *F* centers and empty anion vacancies. Subsequent heating to a temperature range where the vacancies are mobile leads to thermal diffusion of the vacancies and final trapping by *F* centers forming the desired F_2^+ centers.

If the crystals are e^- -irradiated at temperatures where vacancies are mobile and F_2^+ centers are already thermally unstable, only the stable defects will be formed initially. Subsequent cooling into the F_2^+ stability range and light irradiation then produces F_2^+ centers by photoionization of the F_2^+ centers.

1.2.2 Laser-active *F* aggregate centers

Figure (1.4) illustrates the ionic structure and electronic charge distribution of the main laser-active defects in their ground and first excited states. All laser-active defects shown here contain the *F* center as the fundamental building block. They can be categorized as: -

(1) Type II F_A centers, F_A(II). Here the *F* center is attached to a small Li^+ cationic impurity on a <100> nearest-neighbor site.

(2) Type II F_B centers, F_B(II). In this case the *F* center is attached to two <100> neighboring Na^+ cations forming a triangular configuration.

(3) F_2^+ centers – two anion vacancies sharing one electron.

(4) $(F_2^+)_A$ centers – F_2^+ centers attached to a nearest neighbor Li^+ or Na^+ impurity.

(5) (F_2^+)*centers – a defect complex formed from an F_2^+ , a divalent cation impurity and a charge – compensating cation vacancy.

(6) F_A(Tl) centers – an *F* center attached to a <100> neighboring Tl^+ impurity ion having large electron affinity.

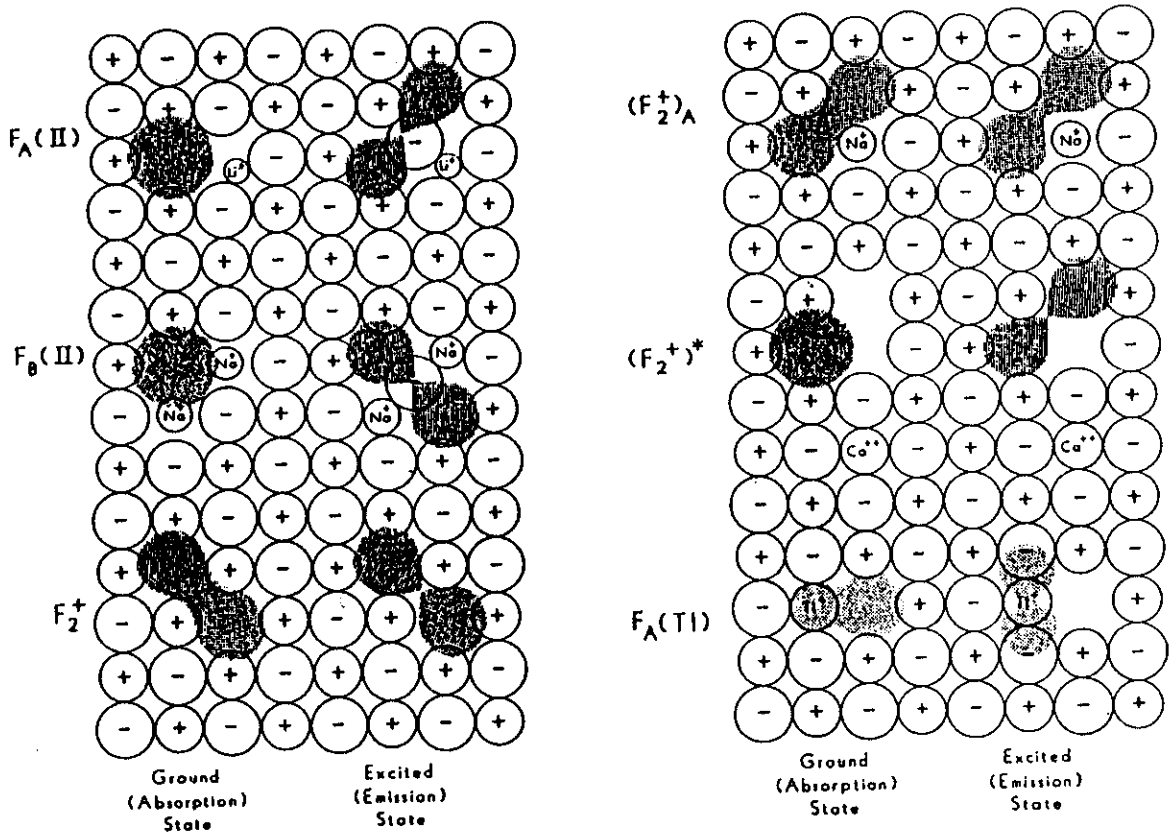

Figure (1.4): Ionic structures of the main laser-active (one electron) *F* aggregate centers, each shown for ground state and excited state configurations. The shaded areas illustrate the electronic charge distributions.

In the following section the main optical properties of some of these defects will be described in more detail.

F_A centers:

F_A centers can be identified as F centers having an alkali metal impurity as a nearest neighbor and therefore presenting a <100> symmetry axis.

An important example for light-induced center formation processes is the aggregation of F centers into F_A centers in the temperature range of anion vacancy mobility, and effect on the absorption spectrum of a Li^+-doped KCl crystal. Starting from an F center system the incoming photon excites the F center electron and causes its transfer, via the conduction band, to another F center, forming temporarily a vacancy with two electrons (F^- center). The empty anion vacancy is mobile and migrates to the Li^+ impurity where it becomes trapped. This complex will finally re-trap the F^- center electron. As a net result the F center system transforms into the F_A center system, as seen in absorption by disappearance of the F band and formation of the two characteristic F_A band after exposure to light.

In F_A centers [38] the threefold degenerate 2p state of the F center is split in absorption Figure (1.5) due to the adjacent cationic impurity, thus forming two well-resolved absorption transitions (F_{A1} band and F_{A2} band). Two types of centers are distinguished corresponding to the different relaxation behavior of the centers after optical excitation.

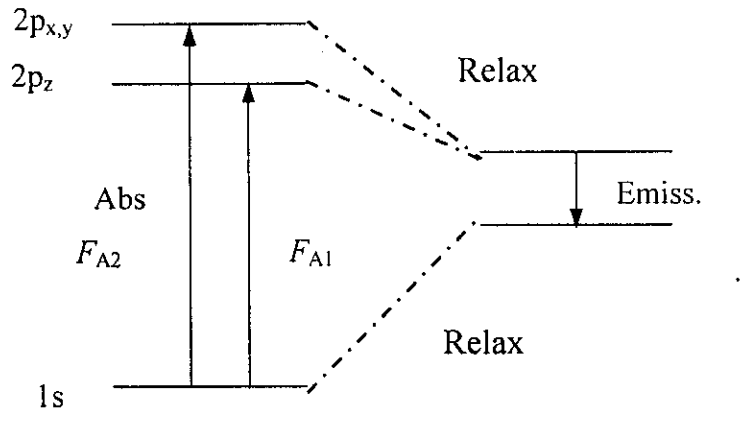

Figure (1.5): Energy level and optical transitions for F_A centers.

In type I F_A centers (*F* centers attached to large size cationic impurities), the emission band from excitation at either of the two absorption components shows a similar stokes shift to that for the *F* centers and the life time is also quite similar.

In type II F_A centers (formed if an *F* center is associated with a small size cationic impurities like Li^+), such as in KCl:Li, the spilitting of the absorption transitions is similar to the type I F_A case but the emission band is very markedly stokes shift and the life time is much shorter than that for the *F* center.

The behavior of the F_A (II) centers has been attributed to the very strong relaxation of the excited state, which causes a nearest neighbor Cl^- to shift to an interstitial position between two adjacent anion vacancies (saddle–point

configuration) in which the electron wave function spreads over the two symmetric wells.

In relation to potential tunable laser applications some effort has been recently devated to the study of *F* centers attached to monovalent cations other than alkali metals, e.g. Ag^+, Ga^+, Tl^+ and In^+. For Tl^+ - doped alkali halides, which are some of the most frequently investigated systems [39,40], it has been concluded that Tl^+ *F* center complexes with the same structure as F_A centers are formed. However, it appears that for the Tl^+ case the bound electron is about equally shared between Tl^+ ion and the anion vacancy. The electronic structure of these non alkali F_A centers appears to be markedly dependent on the electron affinity of the impurity ion.

F_A (Tl) centers:

A previously unknown laser active center was discovered in e^- -irradiated crystals containing Tl^+ impurity [41]. The center formed by optical aggregation of an *F* center to a substitutional Tl^+ impurity, had strong fundamental optical transitions in the near IR between 1 and 2 μm, and was compatible in its polarization behavior with a C_{4v} symmetry defect. Due to its F_A like formation conditions, defect constituents (anion vacancy, <110> neighboring Tl^+ cation and electron) and symmetry properties the defect was termed the F_A (Tl) centers.

The IR wavelength position and small Stokes shift of the fundamental optical transitions indicated that the energy level structure of the F_A (Tl) center had to be quite different from the previously known F_A centers. More specifically, due to the large electron affinity of the Tl^+ impurity, it was proposed that the defect electron had to be at least partially localized at the cationic impurity site [41].

The main optical transitions of the F_A (Tl) centers, identified by the simultaneous growth of the corresponding absorption and emission bands in optical aggregation and thermal annealing steps were measured in seven-host lattices. An experimentally determined energy level diagram of the F_A (Tl) center in KCl is shown in Figure (1.6).

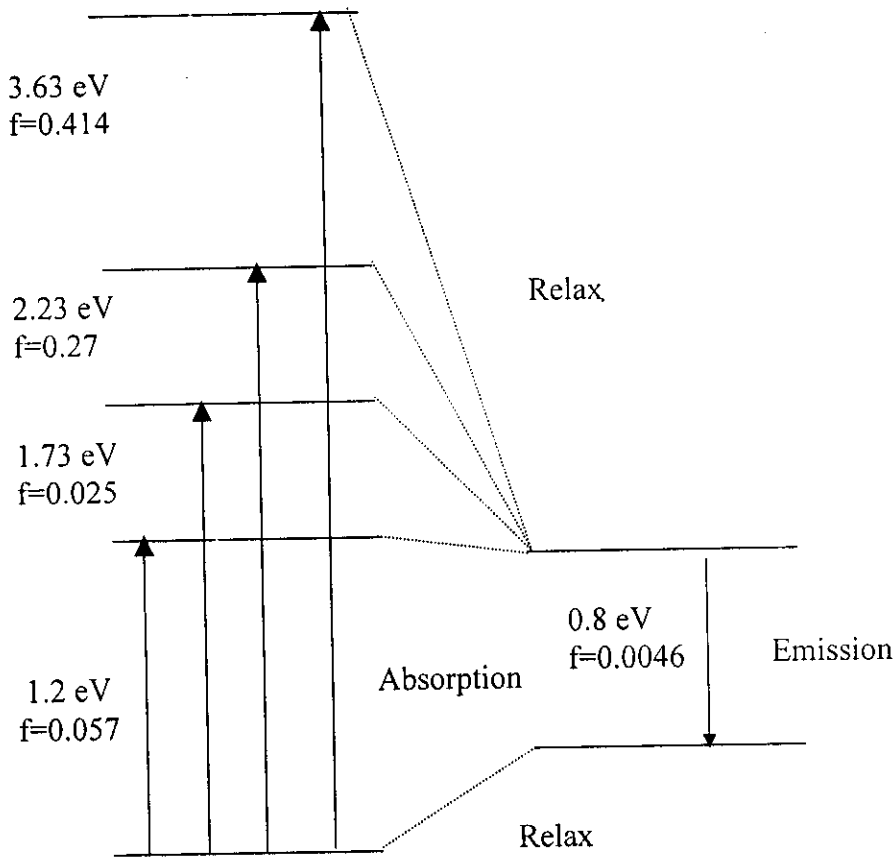

Figure (1.6): Absorption and emission transitions of the F_A (Tl) center in KCl.

positively charged with respect to the lattice they can easily trap and bind an electron-a process which transforms the F_2^+ center into an F_2 center (its neutral counterpart). In order to prevent this destruction, electron traps could be found which trap and bind electrons with higher efficiency than F_2^+ centers. This process achieves by using crystals doped with appropriate amounts of divalent cations like Mn^{+2}, Ni^{+2}, Pb^{+2} [46]. The type of divalent cation which is efficient for electron trapping must be carefully chosen for each host, and the concentration must be kept at a low level to avoid aggregation into larger complexes.

For a full description of F_2^+ center properties a light induced center reorientation process has to be included. Its mechanism was first investigated for the F_2^+ center in KCl [47] and is illustrated in Figure (1.8). If the F_2^+ center in that host is excited from the $1s\sigma_g$ to $2p\pi_u$ level the center performs a subsequent slight relaxation and emits a $2p\pi_u \longrightarrow 1s\sigma_g$ high energy fluorescence in the visible. No center reorientation occurs during this cycle. Above ~ 30 K, however (corresponding to an activation energy of 0.063 eV), the center can be thermally activated from the relaxed excited $2p\pi_u$ state into an H_3^+ molecule-type ionic saddle point configuration with only slightly higher energy. From there a radiationless transition to the $2p\pi_u$ state occurs, connected with a possible reorientation of the center axis. Repeated cycling of the same center through the higher energy states will then lead to its migration through the lattice where it reacts with other defects.

The important conclusion for laser applications of F_2^+ center systems is to avoid exposure of the crystal to light exciting the high energy $1s\sigma_g \longrightarrow 2p\pi_u$ transition, since the highly efficient reorientation (one electron process) will lead to an irreversible center destruction. However, under these precautions some

center destruction, although on a much reduced level, cannot be completely avoided. This was observed in an experiment where only the fundamental absorption of the F_2^+ center was excited then, the F_2^+ center absorption decreased and the same bands observed under excitation of the $1s\sigma_g \longrightarrow 2p\pi_u$ transition were formed again. Obviously, even under excitation of only the low energy transition, the F_2^+ center can be excited in multiple steps from the RES to higher states, finally leading to reorientation and conversion into other defects.

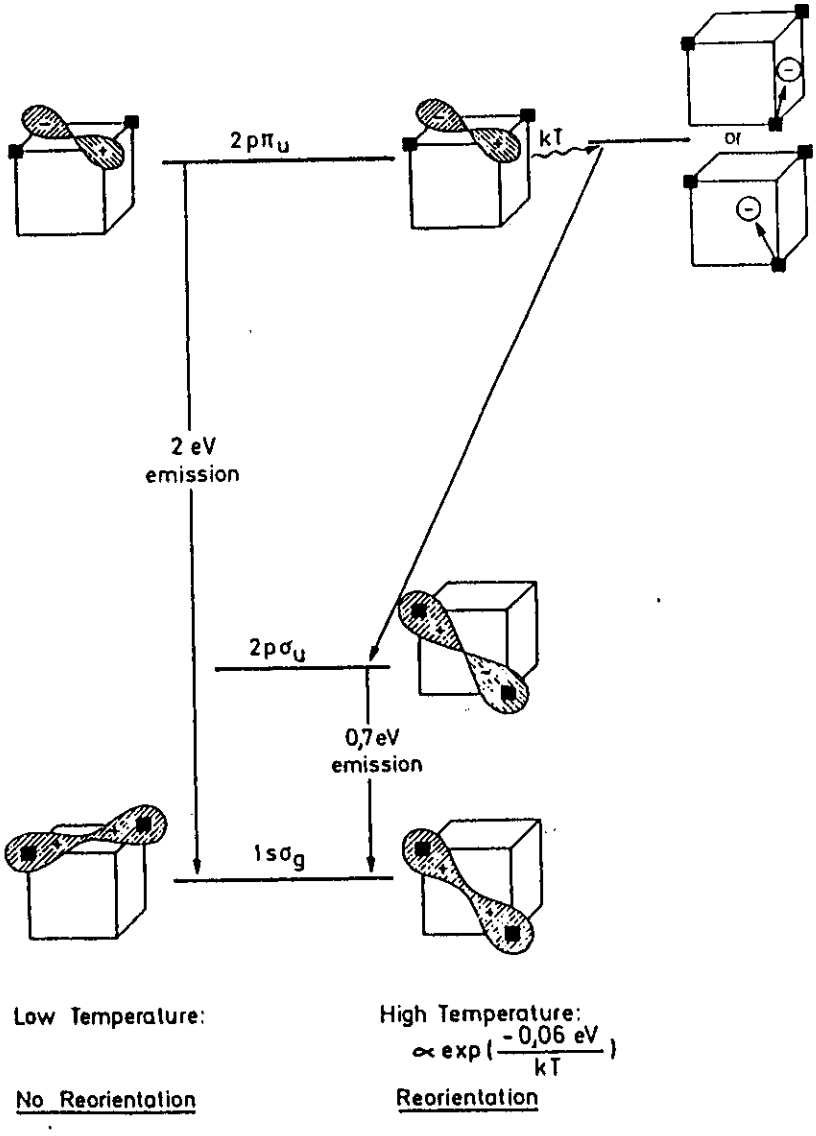

Figure (1.8): Illustration of the lowest electronic states (σ_g, σ_u and π_u) of the F_2^+ center, with indication of the two emission processes and the non-radiative de-excitation processes from the π_u state leading to ionic reorientation.

In order to overcome these fading problems of pure the F_2^+ center systems, defect complexes have been developed in which the F_2^+ centers are bound to neighboring cationic or anionic doping impurities. These F_2^+ like centers retain the F_2^+ energy level structure on a coarse scale, and generally have a higher thermal stability compared with pure F_2^+ centers. In addition, and most important for laser applications, the association to a neighboring impurity stabilizes the position of the F_2^+ center.

1.3 Photographic sensitization

The traditional silver halide photographic process shows promise of flourishing for some time in the future, in spite of the impressive advances that have been made recently in alternative technologies, particularly in electronic imaging. It continues to have some convenience advantages and is still superior in image quality for use in many of the most demanding applications.

It is a remarkable fact that the essential silver halide photosensitive materials of this process have remained the same for more than a century and a half of the dogged pursuit of technological progress in very aspect of human life. During this time great strides have been made in improving the sensitivity, convenience, aesthetic appeal and image quality of the photographic process. These accomplishments have been made without the succession of materials changes that have characterized many other areas of technological advance. Upon close scrutiny it becomes clear that the silver halides possess a number of distinguishing physical properties which, if not individually, are collectively responsible for their unique utility in what turns out to be a highly complex process.

1.3.1 Essentials of the process

After a sheet of photographic film or paper has been exposed to a pattern of light, say in the focal plane of a camera, it is said to bear a *latent image*, which is capable of being converted into a visible image by a photographic *developer*. By absorption of a few quanta of light, some of the light sensitive silver halide crystallites in the film coating have been made susceptible to the action of the developer, the main active ingredient of which is a moderately strong chemical reducing agent. When the exposed film is immersed in this solution, those

crystallites which have absorbed the requisite number of photons quickly begin to be reduced to silver metal whereas those absorbing fewer photons or none are unaffected. Much attention [48] has been given to accurate measurement of absolute sensitivity. Most contemporary results agree that the most efficient commercial camera films require on average about eight to twelve absorbed photons per crystal when exposed under optimum conditions, independent of manufacturer and within limits independent of crystal size. There are films less efficient, but the results seem to confirm that the best do closely approach this range as a limit.

In most black and white films, including radiographic materials and those used for graphic arts, after the residual silver halide is removed, the silver metal constitutes the visible black image. For color films, on the other hand, the silver metal is not part of the final image but instead is dissolved out of the material along with unused silver halide and salvaged for reuse. The colored image consists of dyes formed by reaction of the oxidized developer with organic dye precursor molecules known as couplers. These molecules are ballasted so as not to diffuse out of the coating during processing, and by modifications in the coupler molecule structure, the absorption spectrum of the resulting dye can be controlled to a remarkable degree.

1.3.2 Sensitive materials

Of the four silver halides, the fluoride, chloride, and bromide are sixfold coordinated, with the sodium chloride lattice structure. Silver iodide has fourfold coordination and can exist in two room temperature pseudomorphs: the cubic γ and the hexagonal β forms. Above 147°C (at atmospheric pressure), AgI transforms to the highly conducting α phase.

Silver fluoride is hygroscopic and therefore impractical for photographic use. The photographic characteristics of pure silver iodide have been studied only rarely, partly because of extreme insolubility in aqueous systems and the related problems in its photographic development. Thus silver bromide and silver chloride are the materials that form the basis of the photographic industry. Admixture of a few percent iodide is common, and mixtures of all three halides are occasionally used. In general, camera materials and other high sensitivity films are likely to contain silver bromide, iodide, whereas papers and other low sensitivity materials sometimes also contain effects on photographic response and the chemical reactivities of the products of reduction sensitization are sufficiently different from those of sulphur or sulphur plus gold sensitization that there can be little question that their chemical identities and their sensitizing mechanisms are not the same. Treatment of a coated film with hydrogen gas after previous evacuation is considered by most investigators to be a particular method, perhaps more easily controlled, of reduction sensitization [49].

Some transition metal ions, notably iridium, are moderately effective chemical sensitizers when added during or sometimes after precipitation. Although this sensitization procedure is evidently not used exclusively in any commercial product, it remains a technique of considerable academic interest. Small amounts of iridium or occasionally rhodium or other transition metal ions are sometimes used with conventionally sensitized materials to control the detailed photographic response.

1.3.3 The latent image and photographic development

The questions regarding the nature and mechanism of formation of the photographic latent image have captured the attention of thoughtful practitioners

of the art literally for centuries. Although early literature contained much speculation to the contrary, it is now quite certain that the ultimate effect of the brief exposure is the photoformation of one or more small clusters of silver metal atoms on sufficiently exposed crystallites. These metal clusters promote the further reduction of the host crystallite by the developing agent.

A variety of inorganic and organic species have been found to be suitable developing agents, providing discrimination between exposed and unexposed crystallites. One method that has been used to characterize developing species has been an electrochemical measure of their reduction potential. Although this is by no means the only requirement for a practical developer, it can be generalized that all working ones have reduction potentials in the range between about 60 and 400 mV more reducing than a reference Ag/Ag^+ electrode. A second group of reagents with still higher potential will cause indiscriminate reduction (fog) even without exposure, whereas those with potentials below this range have no effect or may even oxidize existing silver clusters.

1.3.3.1 Lake of development of unexposed crystals

From these measurements it is clear that the reduction of silver ion in contact with any of the practical developers is thermodynamically favored. To understand the catalytic effect of the latent image silver clusters, therefore, it is first necessary to ask what it is that retards the development of unexposed crystals. A description of the phenomena involved [50-51] was formalized by Trautweiler in 1968 and then by Jaenicke in 1972.

The electron from a developer molecule is higher in energy and therefore readily transferred to the lowest vacant 5s orbital of a silver ion in solution. However, when such a silver ion is incorporated into an ionic crystal, all of its

energy levels are raised by several electron volts by virtue of the Madelung potential at the cation site. In the silver halides the vacant 5s level is the origin of the conduction band of the crystal. The conduction band energy minimum is well above the chemical potential range of any non-fogging photographic developer, which falls instead within the forbidden gap of the crystal. Electron transfer to the perfect crystal is therefore energetically unfavourable.

The Fermi energy of metallic silver, on the other hand, lies below the range of chemical potential of working developers and thus transfer to silver metal is favored, as indicated in Figure (1.9). The silver acts simply as an electrode to accept electrons from the developer, transferring them on to defect silver ions not subject to the full Madelung potential. Given sufficient time, even the energetically opposed electron injection into the conduction band of the unexposed crystal can be expected to occur by thermal activation. The consequence of one such injection would be the reduction of one atom of silver, and after a sufficient number of injections the silver so produced would itself act as the catalyst, facilitating injection of subsequent electrons. This is presumably one source of the undesired developed background in unexposed regions, generally known in photographic parlance as *fog*.

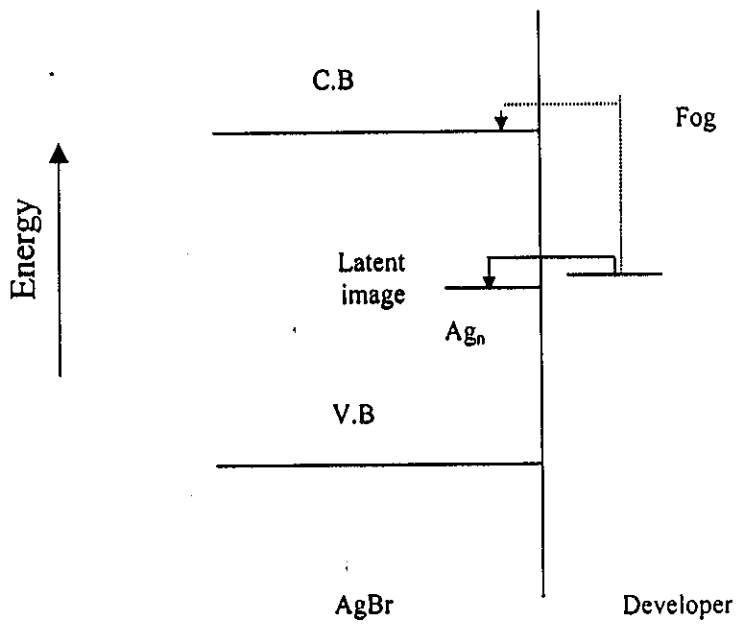

Figure(1.9): The energetics of electron transfer in photographic development. V.B: top of valence band, C.B: bottom of conduction band Ag_n: mettalic cluster.

A variety of observations point to the inescapable conclusion that there is a size requirement for a latent image silver cluster to accept effectively an electron from a developer molecule. The treatments by Trautweiler and Jaenicke also included formal proposals to rationalize these observations. Each suggested that the lowest unfilled energy level of a silver cluster is size dependent, beginning near the silver halide conduction band for the smallest sizes and decreasing progressively toward the bulk Fermi level of silver with increasing size.

With the limited attention that has been directed to metal clusters at the time, both of these authors discussed their models in terms of a monotonic change in energy level with size. It is well recognized that the expected electronic structure of simple clusters of s^1 metal atoms has an alternating aspect, as represented in Figure (1.10). The even sized clusters are characterized by a

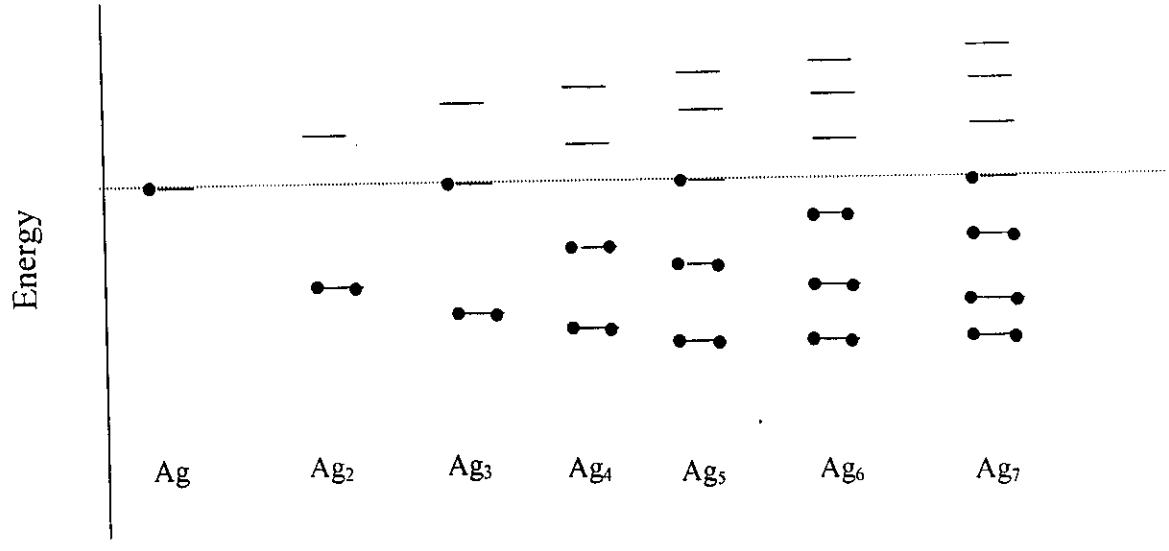

Figure (1.10): A simplified diagram of the developing band of energy levels of a linear chain of s1 atoms with increasing length.

doubly occupied bonding orbital and a higher lying unoccupied antibonding orbital, whereas odd sizes contain a singly occupied orbital at intermediate energy. Measurements of the size dependence of photoionization thresholds of vapour phase clusters have confirmed the alternating concept. Were that also to be the case for photographic clusters, the electron accepting levels would alternate in such a way that all odd sized clusters would easily grow by one atom and that the ultimate developability would always be determined at the even

sizes. The smallest developable size, and indeed all changes in developability, would occur at odd sizes [52].

It is possible, that geometric or steric constraints and/or electronic interactions with the polar supporting crystal might significantly alter this pattern for the s^1 metal clusters of photographic importance. Semi-empirical quantum mechanical calculations [53] with varying degrees of sophisitication have been directed toward this question. The most extensive are those of Baetzold [29], in which models of the defect sites of the support have been included. In his results, the alternating characteristic is retained, though moderated in magnitude from that shown by the isolated clusters [26].

1.4 Computational techniques

1.4.1 Crystal simulation

In cluster calculations, the host surface is represented by only a small number of ions explicitly in the three dimensional space. The remainder may be represented by some long range potential or may be merely ignored [54]. In the early Evjen method [55], the cluster is surrounded by a set of point charges placed in ideal lattice sites. The value of a point charge on the border of this set is 2^{-n}, n being the number of missing nearest neighbors of this charge. More recently the AIMP method has been developed [56] and used by Nygren and Petterson [57] and by Ferrari et al. [58] to embed metal oxide clusters while the rest of the crystal was taken to be full ionic charges. In general, to represent the extended crystal properly, some care needs to be taken in choosing the charges of the point ions, according to the prescription outlined by Harris [59]. For a bulk crystal, the criteria are that there must be no net charge, no net dipole and no net quadruple in the cluster. For a surface, there is a small dipole that is induced by surface rumpling; so the criterion of no net dipole does not hold rigorously [60]. The choice of the appropriate charges for the point ions has been discussed for an FCC structure like MgO [61]. Early studies by Kunz and co-workers [62] and by Colbourn and Mackrodt [63] used clusters that were terminated by full ionic charges. One of the aspects of these calculations (which is most surprising) is that very small clusters - sometimes a single surface ion - can be adequate to represent surface reactivity. This is a consequence of the high degree of localization of the electrons on the ions, and would not hold for materials with any appreciable degree of covalence.

To simulate the low coordinated surfaces of LiH, KCl and AgBr, we follow a procedure previously reported for LiH [8], LiF and NaH [64] and MgO [65]. A finite LiH, KCl and AgBr crystals of 288 point charges were first constructed. The

Coulomb potential along the X and Y axes of these crystals are zero by symmetry as in the host crystals. The charges on the outer shells listed in Table (1.1), were fitted to make the Coulomb potential at the four central sites closely approximates the Madelung potential of the host crystal, and to make the Coulomb potentials at the eight points with coordinates (0,±R,±R) and (±R,0,±R) where R is half the lattice distance, which for LiH, KCl and AgBr, is 2.04, 3.145 and 2.885 Å respectively, equal to zero as it should be in the host crystals. With charges, 0.409283 and 0.800909, the Coulomb potential in the region occupied by the central ions is very close to that in the unit cell of the host crystals. The low coordinated surfaces of the LiH, KCl and AgBr crystals represented in Figure (1.11) were then generated as follows:

1. All charged centers with Cartesian coordinates (±X), (±Y) and ($Z > 0$) were eliminated to generate a flat surface with 176 charged centers occupying the three dimensional space (±X), (±Y) and ($Z \leq 0$).

2. All charged centers with Cartesian coordinates (±X), ($Y > 1$) and ($Z > 0$) were eliminated to generate an edge with 121 charged centers occupying the three dimensional space (±X), ($Y \leq 1$) and ($Z \leq 0$).

3. All charged centers with Cartesian coordinates ($-X < 1$), ($Y > 1$) and ($Z > 0$) were eliminated to generate the H^- and Br^- corners with 81 charged centers occupying the three dimensional space ($-X \geq 1$), ($Y \leq 1$) and ($Z \leq 0$).

The explicitly considered clusters were then embedded within the central region of the crystal surface. All the electrons of the embedded clusters were included in the Hamiltonian of the ab initio calculations. Other crystal sites entered the Hamiltonian either as full or partial ionic charges as demonstrated in Table (1.1).

Table (1.1): Specification of the finite lattices used for flat, edge, and H^-, Br^- corner surfaces of LiH and AgBr as well as flat surface of KCl. R is half the lattice distance, which for LiH, AgBr and KCl is 2.04, 2.885 and 3.145 Å, respectively, and r is the distance of the appropriate shell from the center of the lattice.

	Flat		Edge		H^-, Br^--corner		
r^2/R^2	Coordinates/R (±X), (±Y), (Z ≤ 0)	Number of centers	Coordinates/R (±X), (Y≤ 1), (Z≤0)	Number of centers	Coordinates/R (-X ≥ 1), (Y≤ 1), (Z≤0)	Number of centers	Charge |q|
2	1 1 0	4	1 1 0	4	1 1 0	4	1
6	1 1 2	4	1 1 2	4	1 1 2	4	1
10	3 1 0	8	3 1 0	6	3 1 0	4	1
14	3 1 2	8	3 1 2	6	3 1 2	4	1
18	1 1 4	4	1 1 4	4	1 1 4	4	1
18	3 3 0	4	3 3 0	2	3 3 0	1	1
22	3 3 2	4	3 3 2	2	3 3 2	1	1
26	5 1 0	8	5 1 0	6	5 1 0	4	1
26	3 1 4	8	3 1 4	6	3 1 4	4	1
30	5 1 2	8	5 1 2	6	5 1 2	4	1
34	3 3 4	4	3 3 4	2	3 3 4	1	1
34	5 3 0	8	5 3 0	4	5 3 0	2	1
38	5 3 2	8	5 3 2	4	5 3 2	2	1
38	1 1 6	4	1 1 6	4	1 1 6	4	1
42	5 1 4	8	5 1 4	6	5 1 4	4	1
46	3 1 6	8	3 1 6	6	3 1 6	4	1
50	5 5 0	4	5 5 0	2	5 5 0	1	1
50	5 3 4	8	5 3 4	4	5 3 4	2	1
50	7 1 0	8	7 1 0	6	7 1 0	4	1
54	5 5 2	4	5 5 2	2	5 5 2	1	1
54	3 3 6	4	3 3 6	2	3 3 6	1	1
58	7 3 0	8	7 3 0	4	7 3 0	2	1
66	5 5 4	4	5 5 4	2	5 5 4	1	1
54	7 1 2	8	7 1 2	6	7 1 2	4	0.409293
62	7 3 2	8	7 3 2	4	7 3 2	2	0.409293
66	1 1 8	4	1 1 8	4	1 1 8	4	0.800909
82	9 1 0	8	9 1 0	6	9 1 0	4	0.800909
86	9 1 2	8	9 1 2	6	9 1 2	4	0.800909
		Σ=176		Σ=121		Σ=81	

1.4.2 Calculations

The geometric relaxation of F_A and F_2^+ centers in the ground and excited states is a key quantity for laser activity due to vibronic coupling. In other words, the possible energy level structure of F_A and F_2^+ centers electrons is influenced by the shape and depth of the electronic binding potential. This potential is determined mainly by the distance and geometrical arrangement of the nearest surrounding lattice ions, which oscillate around their equilibrium positions. The ionic equilibrium is different for different electronic states and the electron-phonon coupling and its effect on the optical transitions can be illustrated with the well-known configuration coordinate diagram [32]. In the configuration coordinate diagram, the electronic energies in the ground and excited states are plotted versus the displacement of usually a single configuration coordinate Q which represents a certain localized mode or normal mode of the lattice coupling to the electron. In other words, Q represents the simultaneous inward-outward displacements of the nearest neighbor cations to the defect site(s) from the lattice interionic separation. Starting from the doublet ground state of F_A and F_2^+ an optical excitation produces a transition into the excited states at fixed nuclear coordinates assuming Franck-Condon principle, i.e. vertical in the configuration coordinate diagram. Due to the Gaussian shaped probability function for the lowest vibrational state, the transition starts with the highest probability from the equilibrium position Q_1. The electronic distribution reached after excitation in the excited state is not in equilibrium with the lattice at Q_1. As a consequence the ions oscillate towards new equilibrium position. The vibrational energy will be dissipated via anharmonicity into lattice phonons and the electron-lattice system will reach the new equilibrium position Q_2, the relaxed excited state RES. After the mean life time the excited electron returns to the ground state by a vertical

emission process, and the subsequent lattice relaxation completes the optical cycle [7].

The electron-phonon coupling and its effects on the optical transitions can be illustrated with the well-known configuration coordinate diagram. To construct the configuration coordinate diagrams, the ion clusters representing the F_A center at the flat surfaces of KCl as well as F_2^+ centers at the flat, edge and corner surfaces of LiH and AgBr were first embedded in the three dimensional arrays of point ions described in the subsection (1.4.1). The representation of the ion clusters considered in the calculations for F_A and F_2^+ is given in Figure (1.12) and Figure (1.13) respectively. The absorption and emission energies were then calculated as the difference between the total energies of the ground and the excited states. For this purpose, the relevant potential energy curves were calculated, then according to the Franck-Condon principle the absorption energy was calculated as that for a vertical transition from the minimum of the relaxed ground state to the excited state (with fixed atomic coordinates). The luminescence energy was calculated in a similar manner. Stokes-shifts were then calculated as the difference between absorption and emission energies.

The CI-singles CIS method was employed for the calculations of F_A and F_2^+ tunable laser activities, exciton (energy) transfer and relaxed excited state RES orientational destruction. The CIS method, named CI-singles, uses the configuration interaction approach and model excited states as combinations of single substitutions out of the Hartree-Fock ground state. CI-singles is comparable to Hartree-Fock theory for ground state systems in that it is qualitatively accurate if not always highly quantitatively predictive [66]. Despite this comparison, the CI-singles method does include some electron correlation in the excited states and can provide reasonable accuracy for excitation energies in

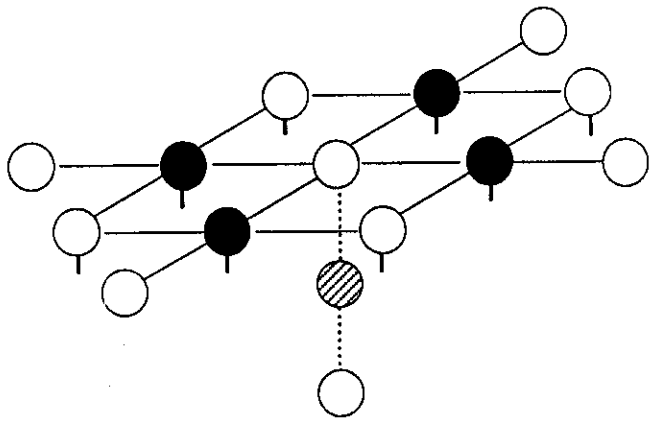

The defect free surface
KCl

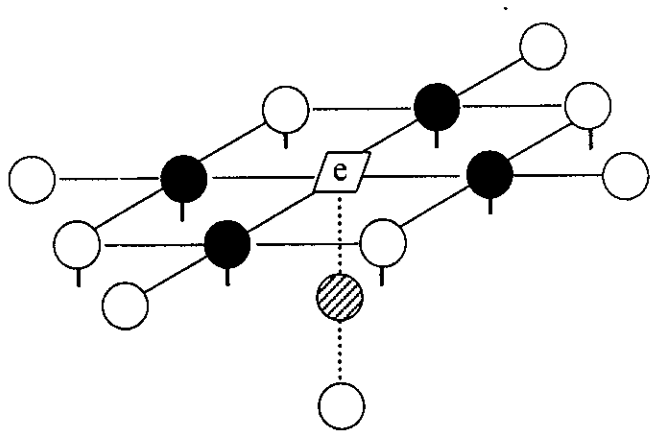

The defect containing surfaces
F_A-K_8Cl_{13}

● : K^+ ○ : Cl^- ▨ : Li^+, Na^+, K^+, Rb^+, Cs^+, Ga^+, In^+, Tl^+ e : F

Figure (1.12): Representation of the defect-free and defect containing surfaces of KCl.

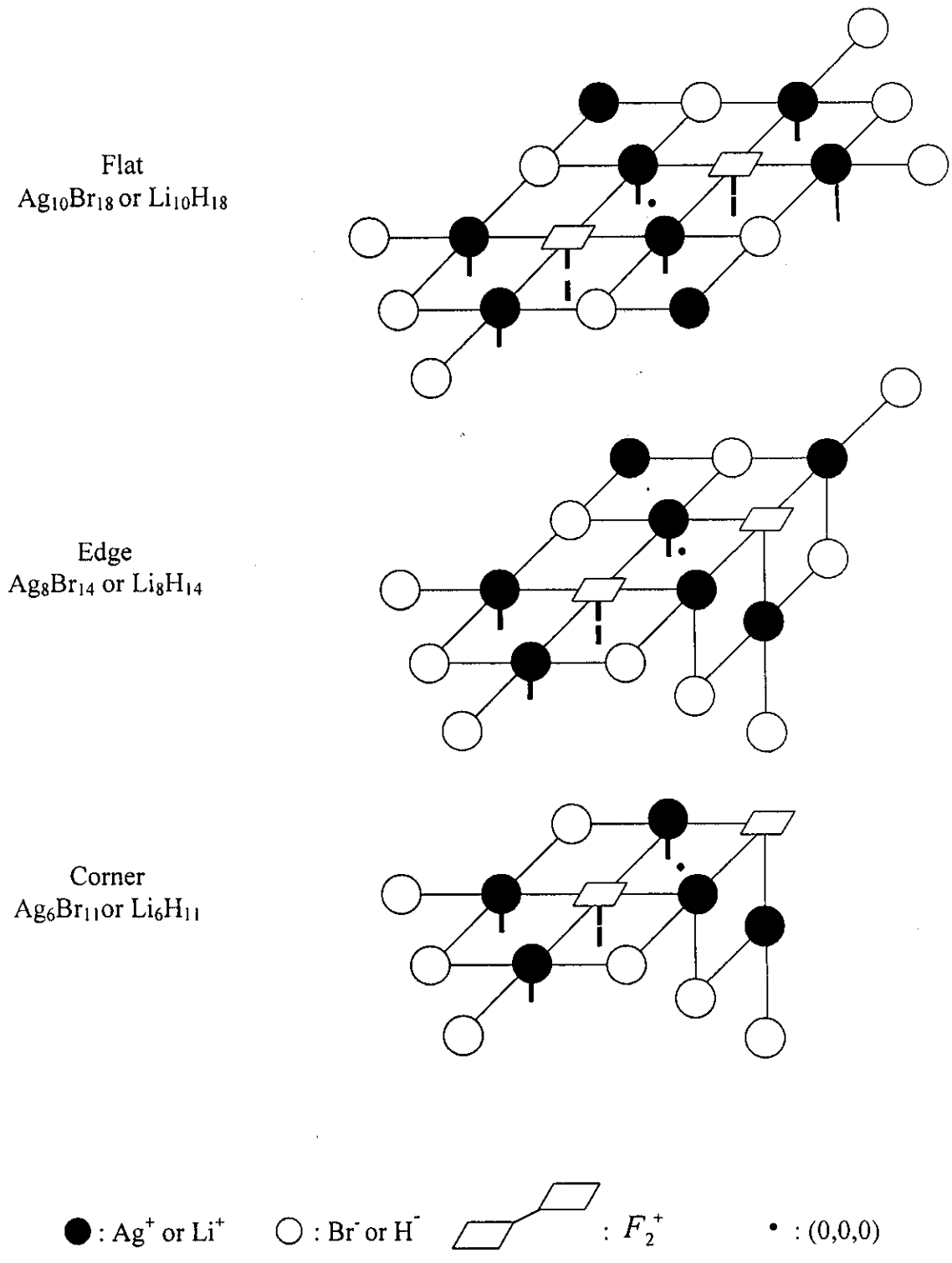

Figure (1.13): Representation of the defect containing surfaces of AgBr and LiH.

comparison with the simplest way to find the lowest relaxed excited state RES in wide gap insulators, namely, the self consistent field calculations of the triplet state [67]. Since the CI-singles is size extensive in the ground state (formally identical to the Hartree-Fock method) and the total electronic energies (rather than the total interaction energies) were calculated, the major sources of errors that might effect the accuracy of the present calculations are the size extensivity error, the basis set superposition error of the adsorbate substrate interactions and the zero point vibrational energy error [68].

The density functional theory (DFT) method was employed for the calculations of F_A and F_2^+ surface relaxation and defect formation energies, the differences between the band gaps and exciton bands (Glasner-Tompkins relation), Mulliken charges and photographic sensitization.

The B3LYP functional is an approximation to the true exchange functional, which has shown to give a good description of interactions involved in the adsorbate-substrate processes [69]. The adsorption energy of the adatom at the substrate surface was calculated from the relation

$$E_{adsorption} = E_{complex} - E_{adsorbate} - E_{substrate} \qquad (1.10)$$

The terms appearing on the right hand side are the total energies of the complex (adsorbate + substrate), the adsorbate and the substrate (defect free or defect containing of LiH and KCl crystals) respectively, obtained from three independent calculations using the same supercell. The negative adsorption energy indicates that the bound adsorbate is electronically stable. The DFT calculations were performed using Becke's three-parameter exchange functional B3 with LYP correlation functional [70]. This hybrid functional includes a mixture

of a Hartree-Fock exchange with DFT exchange correlation. Originally the functional B includes the Slater exchange along with corrections involving the gradient of the density [4] and the correlation functional LYP is that of Lee, Yang and Parr, which includes both local and non-local terms [71]. The Stevens, Basch and Krauss effective core potential CEP basis set [72] was employed in the calculations and the computations were carried out using Gaussian 98 system [73].

The molecular orbitals are expressed as linear combination of a pre-defined set of one-electron functions known as basis functions. These basis functions are usually centered on the atomic nuclei and so bear some resemblance to atomic orbitals [74]. However, the actual mathematical treatment is more general than this, and any set of appropriately defined functions may be used.

An individual molecular orbital is defined as:

$$\Phi_i = \sum_{\mu=1}^{N} c_{\mu i} x_\mu \qquad (1.11)$$

Where the coefficients $c_{\mu i}$ are known as the molecular orbital expansion coefficients. The basis functions $x_1 \ldots x_N$ are also chosen to be normalized. Following the usual notational convention of using roman subscribts on molecular orbital functions and Greek subscripts on basis functions thus, x_μ refers to an arbitrary basis function in the same way that Φ_i refers to an arbitrary molecular orbital.

Ab initio molecular electronic structure programs use Gaussian type for atomic functions as basis functions. Gaussian functions have the general form

$$g(\alpha.., \vec{r}) = cx^n y^m z^l e^{-\alpha r^2} \quad (1.12)$$

Where $\vec{r}$ is composed of x, y, z and α is a constant determining the size (radial extent) of the function. In a Gaussian function, $e^{-\alpha r^2}$ is multiplied by powers (possibly 0) of x, y, z and a constant for normalization, so that:

$$\int_{all\ space} g^2 = 1 \quad (1.13)$$

Thus, c depends on α, l, m and n.

Here, are three representative Gaussian functions (s, p_x, p_y and d_{xy} types, respectively):

$$g_s(\alpha.., \vec{r}) = \left(\frac{2\alpha}{\pi}\right)^{3/4} e^{-\alpha r^2} \quad (1.14)$$

$$g_y(\alpha..., \vec{r}) = \left(\frac{128\,\alpha^5}{\pi^3}\right)^{1/4} ye^{-\alpha r^2} \quad (1.15)$$

$$g_Z(\alpha..., \vec{r}) = \left(\frac{2048\alpha^7}{\pi^3}\right)^{1/4} xye^{-\alpha r^2} \quad (1.16)$$

Linear combination of primitive gaussians like these are used to form the actual basis functions; the latter are called contracted gaussians and have the form:

$$x_\mu = \sum_p d_{\mu p} g_p \tag{1.17}$$

Where the $d_{\mu p}$'s are fixed constants within a given basis set. Note that contracted functions are also normalized in common practice.

All of these constructions result in the following expansion for molecular orbitals.

$$\Phi_i = \sum_\mu c_\mu x_\mu = \sum_\mu c_\mu \left(\sum_\mu d_{\mu p} g_p \right) \tag{1.18}$$

The compact effective core potential CEP basis sets have been employed in the calculations. In these basis sets, the double zeta calcultions are referred to as CEP-31G and the triple zeta calculations are referred to as CEP-121G. However, it may be noted that there is only one CEP basis set defined beyond the second row, and the two basis sets are equivelent for these atoms. For the s-manifold, a quadruple zeta representation of Gaussian type orbitals was found to be necessary to obtain energies with 0.001-0.003 a.u. of large, even-tempered basis set results. For this size expansion, little accuracy was lost by restricting the s- and p- basis sets for each atom to have a common set of expansions. For the d- manifold, a three GTO fits yields eigenfunctions which are <0.001 a.u. different from large, even-tempered results. These potentials and basis sets have been used to calculate the equilibrium structure and spectroscopic properties of several

molecules, and the results compared extremely favorably with corresponding all-electron calculations.

Compact effective potentials, which replace the atomic core electrons in molecular calculations, are represented for atoms in the first and second rows of the periodic table. The angular-dependent components of these potentials are represented by compact one- and two-term Gaussian expansions obtained directly from the appropriate eigenvalue equation. Energy-optimized Gaussian basis set expansions of the atomic pseudo orbitals, which have a common set of exponents (shared exponents) for the s and p orbitals, are also presented. The potentials and basis sets have been used to calculate the equilibrium structures and spectroscopic properties of several molecules. The results compare extremely favorably with corresponding all-electron calculations.

Ab initio effective potentials (EP) are derived from atomic all electron calculations. They are then used in valence only molecular calculations where the atomic cores are chemically inactive. The generation of the EP begins with the atomic Hartree-Fock equation for a valence orbital with angular momentum *l*,

$$\left(-\frac{1}{2}\nabla_r^2-\frac{Z}{r}+\frac{l(l+1)}{2r^2}+V_{val}+V_{core}\right)\Phi_{li}=E_{li}\Phi_{li}. \qquad (1.19)$$

Where V_{core} and V_{val} represent the Coulomb and exchange operators summed over the core and other occupied valence orbitals, respectively. The valence orbital ϕ_{li} is the lowest energy solution of eq. (1.19) only if there are no core orbitals with the same angular momentum. Otherwise the valence orbital must be orthogonal to all lower-energy, core-like solutions of the Hartree-Fock equation, and is therefore noded.

Given solutions of eq. (1.19) obtained from an atomic Hartree-Fock self-consistent field calculation [75], it is possible to use ϕ_{li} and E_{li} to construct a valence-electron-only Hartree-Fock-like equation, which uses an effective potential to ensure that the valence orbital is the lowest energy solution. This equation is written as

$$\left(-\frac{1}{2}\nabla_r^2 - \frac{Z_{eff}}{r} + \frac{l(l+1)}{2r^2} + V_{val} + V_l^{eff}\right)\chi_{li} = E_{li}\chi_{li} \qquad (1.20)$$

Where V_l^{eff} is the effective potential, χ_{li} is a nodeless pseudo orbital that is derived from ϕ_{li} , and E_{li} is the original Hartree-Fock orbital eigenvalue. The effective potential ensures that χ_{li} is the lowest energy solution of eq. (1.20) with eigenvalue E_{li}. Hence, V_l^{eff} replaces the explicit orthogonality constraints of eq. (1.19) as well as the core Coulomb and exchange potentials (V_{core}). Z_{eff} is equal to the nuclear charge minus the number of core electrons.

The effective potential V_l^{eff} must be l dependent, since the core exchange potential and the orthognality conditions are l dependent. However, if the valence orbital angular momentum exceeds the largest l value occuring in the core, there is no radial orthognality constraint and only the core exchange potential requires an l dependence. Since for the first and second row atoms the exchange interaction with the core is small for valence electrons with high angular momenta, the effective potentials for all l values greater than the maximum l occuring in the core are dominated by the core Coulomb potential and are therefore all very similar [72].

The total effective potential for each atom is given by

$$V^{eff}(r) = \sum_{l=0}^{\infty} V_l^{eff}(r) \sum_{m} |lm\rangle\langle lm|, \qquad (1.21)$$

Stevens, Basch and Krauss ECP triple zeta basis set CEP-121+G [72] augmented with polarization and diffuse functions, CEP-31G [72,76-77] and CEP-121G were employed in the calculations. For ionic clusters such as K_9Cl_{14}, $Ag_{10}Br_{20}$ and $Li_{10}H_{20}$ with 112, 340 and 40 interacting electrons respectively, there are 240, 470 and 200 basis functions, as well as 368, 1020 and 300 primitive Gaussians respectively. The numerical computations were carried out using Gaussian 98 system [73].

1.5 Theoretical models

The approximate solution of the Schrödinger equation is achieved by using two broadly different conceptual approaches. In the first approach, each problem is examined at the highest level of theory currently feasible for a system of its size. In the second approach, a level of theory is first clearly defined after which it is applied uniformly to molecular systems of all sizes up to a maximum determined by available computational resources. Such a theory, if prescribed uniquely of electrons, may be termed a theoretical model, within which all structures, energies, and other physical properties can be examined once the mathematical procedure has been implemented through a computer program.

The model may be tested by systematic comparison of its findings with known experimental results. Depending upon such comparison, a model can acquire some predictive value in situations where experimental data are unavailable.

In the following subsections we will discuss the two theoretical methods employed in the thesis, the density functional theory (DFT) and configuration interaction CI-singles.

1.5.1 Density functional theory (DFT)

Density functional theory (DFT) has proved very successful in the past few decades or so in describing the static electronic structure of molecules of considerable size, including such properties as bonding energies, potential surfaces, geometries, vibrational structure and charge distributions. In its original form, however, DFT is essentially confined to ground state properties and the

response of this ground state to static external perturbations such as electric fields. More recently the theory has been generalized to include the effects of time dependent perturbations (such as radiation fields) leading to time dependent density functional theory (TDDFT) which in form looks very similar to time dependent Hartree Fock (TDHF). An extra bonus of TDDFT is that it enables us to calculate excitation energies and oscillator strengths in a consistent way, thus freeing DFT from its ground state limitations. Experience in this area is just building up, but the first results are very encouraging. The method will be extended to the description of periodic systems in one dimension (polymers), two dimensions (surfaces and thin layers) as well as three dimensions (solids). The emphasis is on the linear and non-linear optical properties of these systems as well as their excitation spectra (exciton bands). In the case of surfaces the method also allows the calculation of dispersion interactions between the surface and adsorbate molecules. At a later stage the interaction between the nuclear and electronic degrees of freedom (electron-phonon interaction) has been studied using the same techniques.

In 1964, Hohenberg and kohn [78] proved that the ground state molecular energy, wave function, and all other molecular electronic properties are uniquely determined by the electron probability density ρ (x,y,z), a function of only three variables. The ground state energy E_o is a functional of ρ and writes $E_o = E_o(\rho)$.

If the ground state electron density ρ (x,y,z), has been known, it is possible to calculate all the ground state molecular properties from ρ, first find the wave function Ψ and then find ρ by integration; eq.(1.22)

$\rho(x,y,z)=$

$$n\sum_{all\ m_s}\int\ldots\int\left|\Psi(x,y,z,x_2,\ldots z_n,m_{s1}\ldots,m_{sn})\right|^2 dx_2\ldots dz_n \qquad (1.22)$$

Kohn and Sham [79] showed that the exact ground state purely electronic energy E_o of an n-electron molecule with ground state electron probability density ρ is given by

$$E_0 = -\frac{1}{2}\sum_{i=1}^{n}\left\langle\Psi_i(1)\left|\nabla_1^2\right|\Psi_i(1)\right\rangle - \sum_{\alpha}\int\frac{Z_\alpha\rho(1)}{r_{1\alpha}}dv_1 + \frac{1}{2}\iint\frac{\rho(1)\rho(2)}{r_{12}}dv_1dv_2 + E_{xc}[\rho] \qquad (1.23)$$

Where $\Psi_i(1)$, i = 1,2,...,n , is the Kohn and Sham orbitals, and the exchange-correlation energy $E_{xc}(\rho)$ is a functional of ρ. The notations $\Psi_i(1)$ and $\rho(1)$ indicate that Ψ_i and ρ are taken as functions of the spatial coordinates of electron 1. Kohn and Sham also showed that the exact ground state ρ can be found from the Ψ_i's, according to

$$\rho=\sum_{i=1}^{n}\left|\Psi_i\right|^2 \qquad (1.24)$$

The Kohn - Sham orbitals are found by solving the one electron equations

$$\hat{F}_{ks}(1)\Psi_i(1) = \varepsilon_{i,ks}\Psi_i(1) \qquad (1.25)$$

Where the Kohn - Sham operator $\hat{F}_{ks}$ is

$$\hat{F}_{ks} = -\frac{1}{2}\nabla_1^2 - \sum_{\alpha}\frac{Z_\alpha}{r_{1\alpha}} + \sum_{j=1}^{n}\hat{J}_j(1) + V_{xc}(1) \qquad (1.26)$$

Where the Coulomb operator $\hat{J}_j(1)$ is defined by

$$\hat{J}_j(1)f(1) = f(1)\int|\Phi_j(2)|^2\frac{1}{r_{12}}dv_2 \qquad (1.27)$$

Where f is an arbitrary function, $|\Psi_j(2)|^2$; is the electron density, and the exchange-correlation potential V_{xc} is found as the functional derivative of E_{xc}:

$$V_{xc} = \delta E_{xc}(\rho)/\delta\rho \qquad (1.28)$$

If $E_{xc}(\rho)$ is known, its functional derivative is readily found, and so V_{xc} is known. $\hat{F}_{ks}$ is like the Hartree-Fock operator, except that the exchange operators $-\sum_{j=1}^{n}\hat{k}_j$ are replaced by V_{xc}, which contain the effects of both exchange (antisymmetry) and electron correlation.

For a closed shell ground state, the electrons are paired in the Kohn - Sham orbitals, with two electrons of opposite spin having the same spatial Kohn - Sham orbital.

Substitution of eq.(1.26) in (1.25) and use of (1.27) gives

$$\left(-\frac{1}{2}\nabla_1^2 - \sum_{\alpha}\frac{Z_\alpha}{r_{1\alpha}} + \int\frac{\rho(2)}{r_{12}}dv_2 + V_{xc}(1)\right)\Psi_i(1) = \varepsilon_{i,ks}\Psi_i(1) \qquad (1.29)$$

There is only one restriction in using the Kohn – Sham equations to find ρ and E: no one knows what the correct functional $E_{xc}(\rho)$ is for molecules.

Various approximate functions $E_{xc}(\rho)$ have been used in molecular DF calculations. To investigate the accuracy of a particular approximate $E_{xc}(\rho)$, it can be used in DF calculations and compares the calculated molecular properties with their experimental values.

If ρ varies very slowly with position, one can show that $E_{xc}(\rho)$ is given by

$$E_{xc}^{LDA}(\rho) = \int\rho(x,y,z)\varepsilon_{xc}(\rho)dxdydz \qquad (1.30)$$

Where the integral is over all space and $\varepsilon_{xc}(\rho)$ is the exchange plus correlation energy per electron in a homogeneous electron gas with electron density ρ. A homogeneous electron gas is a hypothetical electrically neutral, infinite volume system consisting of an infinite number of electrons moving in a space throughout which positive charge is continuously and uniformly distributed; the number of electrons per unit volume has a nonzero value ρ.

In a molecule, the positive charge is not uniformly distributed, but is located only at the nuclei. Hence, ρ varies rapidly in a molecule, and eq. (1.30) is only an approximation when applied to molecules, an approximation called the local density approximation (LDA). Molecular LDA calculations show only fair agreement with experimental molecular properties. Much better results are obtained with an improved version of the LDA called the local spin density

approximation (LSDA); the LSDA uses different orbitals and different densities ρ^{α} and ρ^{β} for electrons with different spins.

How dose one do a DF calculation with E_{xc}^{LDA} ? Starting with an initial guess for ρ, eq. (1.28) can be used with $E_{xc} = E_{xc}^{LDA}$ to find an initial V_{xc} , which is then used in (1.29) to find an initial set of Kohn - Sham orbitals Ψ_i . The initially found Ψ_i's are used in eq.(1.24) to get an improved ρ, which is then used to find an improved V_{xc}, which is used to find improved Ψ_i's, and so on. Once the calculation has converged, E_o is found from eq. (1.23) using the converged ρ and E_{xc}^{LDA} . The dipole moment can be calculated from ρ using eq. (1.31)

$$d = -e\int\int\int \rho(x,y,z) r \, dxdydz + e\sum_{\alpha} Z_{\alpha} r_{\alpha} \qquad (1.31)$$

Where r_{α} is the vector from the origin to the nucleus of atomic number Z_{α} and r = xi + yj + zk and similarly for other one electron properties. For large molecules, DF calculations are faster than SCF calculations [80].

Another commonly used version of the density functional method is the X_{α} method (the X stands for exchange). Here, the correlation contribution to E_{xc} is neglected and (based on the homogeneous electron gas model) the exchange contribution is taken as

$$E_{x\alpha} = -\frac{9}{8}\left(\frac{3}{\pi}\right)^{1/3} \alpha \iiint \rho^{4/3}(x,y,z)\ dxdydz \qquad (1.32)$$

Where α is an adjustable parameter; values of α from 2/3 to 1 have been used. Functional differentiation of $E_{x\alpha}$ yields the X_α exchange potential as $V_{x\alpha} = -(3\alpha/2)(3\rho/\pi)^{1/3}$. The X_α eq. (1.29) with V_{xc} replaced by $V_{x\alpha}$ can be solved by expansion of the Ψ_i's using a basis set, but this requires a lot of computation. A much more efficient procedure is to solve the X_α equations numerically, using the following technique.

One divides space into several regions by imagining a sphere around each atom and a larger sphere around the entire molecule. Within each atomic sphere, and in the region outside of the molecular sphere, the potential energy terms in eq. (1.29) are averaged over the angles θ and φ so as to produce a spherically symmetric potential energy in each of these regions; in the interstitial region between the atomic spheres and within the molecular sphere, the potential energy is assumed constant. Within each atomic sphere, one uses an α value appropriate to that atom; these are taken as the α values needed for an X_α calculation on the isolated atom to produce an energy equal to the Hartree-Fock energy of that atom.

The X_α method was originally developed by Slater for atoms and is sometimes called the Hartree-Fock-Slater method, since it was viewed as providing an approximation to the Hartree-Fock method. However, the X_α method is best viewed as a special case of the density functional method, and not as an approximate Hartree-Fock theory; for example, the orbital energies obtained in the X_α method donot give good approximations to the energies needed to remove

an electron from each of the MOs and differ substantially from SCF orbital energies [81].

1.5.2 Configuration interaction (CI-singles)

We begin by selecting the Hartree-Fock single-determinantal wave function, Ψ_{HF}, as a reference for the ground state of the system:

$$\Psi_{HF} = (n!)^{-1/2} \det \{\chi_1 \chi_2 \ldots \chi_i \chi_j \ldots \chi_n\} \quad (1.33)$$

Where n is the number of electrons and χ_p are spin orbitals represented in a convenient basis of N atomic basis functions, Φ_μ :

$$\chi_p = \sum_{\mu}^{N} C_{\mu p} \Phi_\mu \quad (1.34)$$

In principle, this reference state need not be the ground state but could be any excited HF state as well. The following subscript notation will be used throughout: $\mu,\upsilon,\lambda,\sigma,\ldots$, denote atomic basis functions; i , j, k, l, ..., denote molecular orbitals which are occupied in the ground state; a ,b ,c ,d ,...,.denote virtual molecular orbitals, unoccupied in the ground state ; p, q, r, s,..., denote generic molecular spin orbitals. The molecular orbital coefficients, $\{C_{\mu p}\}$, are easily determined by standard self consistent field (SCF) procedures which solve the Hartree-Fock equations:

$$\sum_{\mu} (F_{\mu\upsilon} - \varepsilon_P S_{\mu\upsilon}) C_{\upsilon p} = 0 \quad (1.35)$$

Here $F_{\mu\upsilon}$ represents the Fock matrix:

$$F_{\mu\upsilon} = H_{\mu\upsilon} + \sum_{\lambda\sigma} \sum_{i} C_{\mu i} C_{\upsilon i} (\mu\lambda \,||\, \upsilon\sigma) \quad (1.36)$$

given in terms of the one-electron core Hamiltonian, $H_{\mu\upsilon}$ and the usual antisymmetrized two electron integrals:

$$(\mu\nu||\lambda\sigma) = \iint \Phi_\mu(1)\,\Phi_\nu(2)\left(1/r_{12}\right)\left[\Phi_\lambda(1)\,\Phi_\sigma(2) - \Phi_\sigma(1)\,\Phi_\lambda(2)\right] dr_1 dr_2 \quad (1.37)$$

$S_{\mu\upsilon}$ represents the overlap matrix:

$$S_{\mu\nu} = \int \Phi_\mu \Phi_\nu \, dt \quad (1.38)$$

and ε_P is the one-electron energy of orbital p. in these expressions, we have assumed real orbitals throughout. After these equations are solved, the total energy of the ground state single determinant can be expressed as

$$E_{HF} = \sum_{\mu\nu} P^{HF}_{\mu\nu} H_{\mu\nu} + \frac{1}{2} \sum_{\mu\nu\lambda\sigma} P^{HF}_{\lambda\sigma} P^{HF}_{\mu\nu} (\mu\lambda\|\nu\sigma) + V_{nuc} \quad (1.39)$$

Where P^{HF} is the HF density given as a sum over the occupied orbitals:

$$P^{HF}_{\mu\upsilon} = \sum_{i=1}^{n} C_{\mu i}\, C_{\upsilon i} \quad (1.40)$$

and V_{nuc} is the nuclear repulsion energy. eq. (1.33) represents only one of several possible determenants for an electronic wave function of the system. Consider the n(N-n) possible singly excited determinants made by replacing an occupied spin orbital with a virtual spin orbital. Such wave functions and associated energies can be written

$$\Psi_{ia} = (n!)^{-1/2} \det \{\chi_1 \chi_2 \ldots \chi_a \chi_j \ldots \chi_n\} \quad (1.41)$$

$$E_{ia} = E_{HF} + \varepsilon_a - \varepsilon_i - (ia \,||\, ia) \tag{1.42}$$

Where we have introduced the antisymmetrized two-electron integrals in the molecular orbital basis:

$$\langle pq \,\|\, rs \rangle = \sum_{\mu\nu\lambda\sigma} C_{\mu p} C_{\nu q} C_{\lambda r} C_{\sigma s} \langle \mu\nu \,\|\, \lambda\sigma \rangle \tag{1.43}$$

These singly excited wave functions and energies (STA) can be considered first approximations to the molecular excited states of the system. Disadvantages in using eq. (1.41) as a wave function are well-known: (1) It is not an eigenfunction of the spin-squared operator and therefore does not yield pure spin states for closed-shell systems. (2) The spin orbitals involved in the transition have been variationally determined for the ground state. Forcing the virtual orbital to be occupied is more closely related to ionization rather than excitation. (3) It is not at all appropriate for excitations into degenerate spin orbitals. For instance, the π to π* excited states of benzene can be understood only as a mixture of four singly excited determinants.

These objections are partially overcome if the excited state wave function is written as a linear combination of all possible singly excited determinants:

$$\Psi_{CIS} = \sum_{ia} a_{ia} \Psi_{ia} \tag{1.44}$$

These configuration interaction (CI) coefficients can be deduced as normalized eigenvectors of the Hamiltonian matrix:

$$\langle \Psi_{ia} | H | \Psi_{jb} \rangle = [E_{HF} + \varepsilon_a - \varepsilon_i]\ \delta_{ij}\delta_{ab} - (ja \| ib) \qquad (1.45)$$

We refer to this procedure as full configuration interaction in the space of single substitutions or " CI singles ". Eigenvalues, E_{CIS}, of eq. (1.45) are the CI-singles total energies for various excited states. Several points should be made: (1) Ψ_{CIS} is properly orthogonal to the ground-state Ψ_{HF} :

$$\langle \Psi_{ia} | H | \Psi_{HF} \rangle = 0 \qquad (1.46)$$

(2) The variational determination of the CI-singles coefficients allows the overall wave function to relax so that Ψ_{CIS} more properly represents an excited state rather than an ionized state; (3) for closed-shell systems, it is possible for Ψ_{CIS} to describe pure sign singlets and triplets (no spin contamination) by allowing positive and negative combinations of α and β excitations from one doubly occupied orbital to one virtual orbital; (4) CI-singles leads to a well-defined wave function and differentiable energy, thus analytical gradient techniques to determine properties and optimized excited-state geometries are straightforward to apply; (5) CI-singles is also a size-consistent method [82].

1.5.2.1 Determining the analytical first derivative of the CI-singles energy

Schemes, which evaluate the gradient of generic CI energies have been available for several years. Indeed, simple modifications of existing programs can be used to generate the gradient of the CI-singles energy. Our emphasis in this

section is on the algebraic manipulation of the terms needed for the present case. The simplicity of this special case leads to a technique which will make the computation of excited-state properties for large molecules feasible.

The total energy for a CI-singles excited state is an eigenvalue of the matrix given in eq. (1.45). It can be written as

$$E_{CIS} = E_{HF} + \sum_{ia} a_{ia}^2 (\varepsilon_a - \varepsilon_i) - \sum_{ijab} a_{ia} a_{jb} (ja \| ib) \qquad (1.47)$$

The first derivative of E_{CIS} with respect to any external system parameter (for example, a geometric variable or an applied electric field) can be written

$$E_{CIS}^{x} = E_{HF}^{x} + \sum_{ia} a_{ia}^2 (\varepsilon_a^x - \varepsilon_i^x) -$$

$$\sum_{ijab} a_{ia} a_{jb} \left[(j^x a \| ib) + (ja^x \| ib) + (ja \| i^x b) + (ja \| ib^x) \right] \qquad (1.48)$$

Where the superscript x refers to differentiation of the given term with respect to that parameter. The diagonalization of eq. (1.45) ensures that there are no terms involving CI coefficient derivatives. The first term of eq. (1.48) is handled by ordinary HF derivative theory [83], while the remaining terms require the knowledge of first order changes in the Fock and overlap matrices

$$\varepsilon_P^x = F_{PP}^x - S_{PP}^x \varepsilon_P \qquad (1.49)$$

Molecular orbital (MO) coefficient derivatives

$$C_{\mu p}^x = \Sigma_q C_{\mu q} U_{qp}^x \qquad (1.50)$$

as well as two-electron integral derivatives. The MO coefficient derivatives emerge as by products of solving the coupled-perturbed Hartree-Fock (CPHF) equations [84] for the unknown *U* matrix

$$\sum_{ia}[1-A_{ijab}]U^{x}_{ia} = \frac{O^{x}_{ih}}{\varepsilon_j - \varepsilon_b} \qquad (1.51)$$

Where Q_{jb} is a perturbation-dependent quantity and A_{ijab} is a matrix involving transformed two-electron integrals:

$$A_{ijab} = \frac{(ab||ij)+(aj||ib)}{\varepsilon_j - \varepsilon_a} \qquad (1.52)$$

The presence of Q_{jb} in eq. (1.51) implies that the linear equations must be solved separately for each variable in the perturbation (one for each geometric degree of freedom in a geometry optimization). Evaluation of the gradient could proceed in this manner, except that it would be extremely inefficient. Our implementation involves several general enhancements that have been suggested by others. First, we follow the realization of Handy and Schaefer [85] that only one perturbation-independent CPHF equation needs to be solved. Second, in the spirit of Rice and Amos [86] we seek to derive an equation which does not require the transformation of the atomic orbital derivative integrals (a task which has been shown to be cumbersome and unnecessary).

We can recast the CI-singles gradient in the following form:

$$E^{x} = \sum_{\mu\nu\lambda\sigma} \Gamma^{CIS}_{\mu\nu\lambda\sigma}(\mu\nu|\lambda\sigma)^{x} + \sum_{\mu\nu} P^{CIS}_{\mu\nu} H^{x}_{\mu\nu} + \sum_{\mu\nu} W^{CIS}_{\mu\nu} S^{x}_{\mu\nu} + V^{x}_{nuc} \qquad (1.53)$$

The first term in eq. (1.53) involves the contraction of the two-particle CI-singles density matrix with two-electron integral derivatives. The second term involves the contraction of the CI-singles density matrix with the one-electron Hamiltonian derivatives. The third term is the contraction of an "energy-weighted " density matrix with the overlap integral derivatives. The final term is the nuclear repulsion energy derivative. The important construct here is the fact that all multiplications are performed in the atomic orbital (AO) basis. This suggests that one possible algorithm would begin by evaluating the Γ^{CIS}, P^{CIS}, and W^{CIS} matrices as preliminary quantities and then producing the gradient by a simple contraction with derivative integrals of the atomic orbitals. These derivative integrals could be stored on disk or generated as needed (in the usual sense of a direct calculation).

The two particle CI-singles density matrix, Γ^{CIS}, can be written in terms of the HF ground-state density matrix and the ground to excited state transition density matrix, T^{CIS}.

$$\Gamma^{CIS}_{\mu\upsilon\lambda\sigma} = 1/2[P^{HF}_{\mu\upsilon} P^{HF}_{\lambda\sigma} + 2\, T^{CIS}_{\mu\upsilon} T^{CIS}_{\lambda\sigma} - P^{HF}_{\mu\sigma} P^{HF}_{\lambda\upsilon} - 2\, T^{CIS}_{\mu\sigma} T^{CIS}_{\lambda\upsilon}] \tag{1.54}$$

P^{HF} is given in eq. (1.40) while T^{CIS} can be expressed

$$T^{CIS}_{\mu\upsilon} = \sum_{ia} a_{ia} C_{\mu i} C_{\upsilon a} \tag{1.55}$$

The CI-singles excited state density matrix, P^{CIS}, is also constructed as a sum of HF and excited state terms:

$$P^{CIS}_{\mu\upsilon} = P^{HF}_{\mu\upsilon} + P^{\Delta}_{\mu\upsilon} \tag{1.56}$$

Here we have introduced P^{Δ}, the CI-singles Δ density matrix. This can also be called a "difference density matrix", since it represents the changes in electronic distribution upon excitation. It is not however, the same as the transition density matrix defined above. Identification and evaluation of this Δ density matrix is an important step in calculating accurate excited state properties using the CI-singles framework. As we shall demonstrate, it is the use of the true CI-singles density matrix required by eq. (1.53), which allows the realistic computation of charge distributions, orbital populations and electronic moments of the excited state. In the MO basis, it is a symmetric matrix with both occupied-occupied (OO) and virual-virual (VV) contributions:

$$P^{\Delta}_{ij} = -\sum_{ab} a_{ia} a_{jb} \tag{1.57}$$

$$P^{\Delta}_{ab} = +\sum_{ij} a_{ia} a_{jb} \tag{1.58}$$

With the occupied-virual (OV) elements all zero. The true CI-singles density matrix required in eq. (1.53) will have exactly the same OO and VV contributions, but the OV terms are not all zero. The appearance of these off-diagonal block elements in the excited state density matrix can be interpreted as orbital relaxation following the initial gross charge rearrangement due to excitation. That is to say, the CI coefficients will by themselves describe some of the gross features of charge redistribution in the excited state, but the response of the wave function to an external perturbation will account for further refinement in electronic properties. These OV terms can be found by solving a single set of CPHF equations:

$$L_{ai} = \sum_{bj} [(ij||ab)-(ib||ja)] P^{\Delta}_{bj} + (\varepsilon_a - \varepsilon_i) P^{\Delta}_{ai} \tag{1.59}$$

Where the L vector is the CI-singles Lagrangian:

$$L_{ai} = C1_{ai} - C2_{ai} + \sum_{kl} P^{\Delta}_{kl}(al||ik) + \sum_{bc} P^{\Delta}_{bc}(ab||ic) \quad (1.60)$$

$$C1_{ai} = -2 \sum_{jab} a_{ia}a_{jb}(cb||ja) \quad (1.61)$$

$$C2_{bk} = -2 \sum_{ija} a_{ia}a_{jb}(ik||ja) \quad (1.62)$$

It should be noted that the solution of eq. (1.59) as implemented Gaussian-90 does not require the transformed two-electron integrals to be stored on disk. The appropriate matrix multiplication can be performed in a"direct" fashion, using stored two-electron integrals or regeneration of them each interaction. The total CI-singles Δ density matrix required in eq.(1.56) can be generated by transforming the entire MO basis Δ density matrix defined by eqs. (1.57),(1.58) and (1.59).

$$P^{\Delta}_{\mu\upsilon} = \sum_{pq} P^{\Delta}_{pq} C_{\mu p} C_{\upsilon q} \quad (1.63)$$

The final term in the CI-singles gradient requires the energy weighted density matrix. This is also a sum of HF and excited-state terms

$$W^{CIS}_{\mu\upsilon} = W^{HF}_{\mu\upsilon} + W^{\Delta}_{\mu\upsilon} \quad (1.64)$$

The first term has been presented in [82]:

$$W^{HF}_{\mu\upsilon} = \sum_{i} \varepsilon_i C_{\mu i} C_{\upsilon i} \quad (1.65)$$

While the second term can be shown to have OO,VV, and OV contributions in the MO basis:

$$W^{\Delta}_{ij} = -p^{\Delta}_{ij}\,\varepsilon_i - S1_{ij} - \sum_{pq} p^{\Delta}_{pq}(ip||jq) \qquad (1.66a)$$

$$W^{\Delta}_{ab} = p^{\Delta}_{ab}\,\varepsilon_a - S2_{ab} \qquad (1.66b)$$

$$W^{\Delta}_{ai} = -C2_{ai} - p^{\Delta}_{ai}\,\varepsilon_i \qquad (1.66c)$$

Here the only new quantities are the S matrices:

$$S1_{ij} = \sum_{ab} a_{ia} b_{jb} \qquad (1.67a)$$

$$S2_{ab} = \sum_{ij} a_{ia} b_{jb} \qquad (1.67b)$$

Which involve the product vector

$$b_{jb} = -\sum_{ia} a_{ia}(ja||ib) \qquad (1.68)$$

transformation of this matrix to the AO basis for use in (1.64) is straightforward :

$$W^{\Delta}_{\mu\upsilon} = \sum_{pq} W^{\Delta}_{pq} C_{\mu p} C_{\upsilon q} \qquad (1.69)$$

1.5.2.2 Correlated treatment for excited states.

Having suggested the CI-singles level of theory as an adequate zero-order approximation to many excited states, it would be useful to have an additional expression which attempts to access what influence the mixing in of other determinants has on the energy and properties of the excited state. These effects might be included in a manner similar to the ground state correlation correction given by Møller-plesset perturbation theory. Recall that for a HF state, the

second-order perturbation correction (MP2) to the energy involves a summation over matrix elements between the zeroth-order state and doubly substituted determinants from that state:

$$\Delta E_{MP2} = -\sum_{S}^{doubles} \frac{\left\langle \Psi_{HF} | H | \Psi_S \right\rangle^2}{E_S - E_{HF}} = -1/4 \sum_{ijab} \frac{(ij||ab)^2}{\varepsilon_a + \varepsilon_b - \varepsilon_i - \varepsilon_j} \qquad (1.70)$$

This summation runs over single substitutions as well, but according to eq. (1.46) those matrix elements will all be zero. This suggests that if the zeroth-order wave function is a CI-singles eigenvector, a second-order correction will again involve single and double substitutions from the reference state. This implies that it should involve doubles and triples from the ground state. One way in which this interaction might be determined is through the following algebraic expression:

$$\Delta E_{CIS\text{-}MP2} = -1/4 \sum_{ijab} \frac{\left\langle \Psi_{CIS} | H | \Psi_{ijab} \right\rangle^2}{\varepsilon_a + \varepsilon_b - \varepsilon_i - \varepsilon_j - \Delta_{CIS}} \cdot$$

$$1/36 \sum_{ijkabc} \frac{\left\langle \Psi_{CIS} | H | \Psi_{ijkabc} \right\rangle^2}{\varepsilon_a + \varepsilon_b + \varepsilon_c - \varepsilon_i - \varepsilon_j - \varepsilon_k - \Delta_{CIS}} \qquad (1.71)$$

Here Δ_{CIS} is the CI-singles excitation energy, E_{HF}-E_{CIS}. It is important to note that this expression is not derivable from standard perturbation theory but is simply suggested as one way to access the influence of higher determinants on the CI-singles energy. The numerators of eq. (1.71) are given by a linear transformation of the CI-singles amplitudes:

$$\left\langle \Psi_{CIS} \left| H \right| \Psi_{ijab} \right\rangle = \sum_{ib} a_{ib} \left\langle \Psi_{CIS} \left| H \right| \Psi_{ijab} \right\rangle = u_{ijab} \quad (1.72)$$

$$\left\langle \Psi_{CIS} \left| H \right| \Psi_{ijkabc} \right\rangle = \sum_{ib} a_{ib} \left\langle \Psi_{CIS} \left| H \right| \Psi_{ijkabc} \right\rangle = u_{ijkabc} \quad (1.73)$$

these u vectors can be thought of as correction amplitudes for doubly and triply substituted determinants. They have been derived previously [87] and are used in other correlated methods:

$$u_{ijab} = \sum_{c} [(ab||cj)a_{ic} - (ab||ci)a_{jc}] + \sum_{k} [(ka||ij)a_{kb} - (kb||ij)a_{ka}] \quad (1.74)$$

$$u_{ijkabc} = a_{ia}(jk||bc) + a_{ib}(jk||ca) + a_{ic}(jk||ab) + a_{ja}(ki||bc) + a_{jb}(ki||ca) + a_{jc}(ki||ab) + a_{ka}(ij||bc) + a_{kb}(ij||ca) + a_{kc}(ij||ab) \quad (1.75)$$

The quantity in eq. (1.71) can be added to E_{CIS} to define a second-order total energy for an excited state, $E_{CIS\text{-}MP2}$ and the entire procedure can be referred to as CI-singles MP2 theory. The size consistency of this energy is easily justified from the fact that elements of the u vectors will be zero unless all of their subscripts correspond to orbitals localized on the same fragment. The method is, however, nonvariational. A corrected excitation energy can be calculated by taking the difference in this energy from the ground-state MP2 energy.

1.5.2.3 Computational considerations

In this section we summarize some of the algebraic and algorithmic details of the CI-singles calculation with particular emphasis on the feasibility and efficiency of direct methods (those requiring no disk storage of two electron

integrals). To diagonalize the singles matrix of eq.(1.45), the most computationally demanding step in the Davidson procedure [88] is the vector multiplication of a trial CI-singles vector with the Hamiltonian, shown in eq. (1.68). This is easily accomplished if the two electron repulsion integrals from an SCF calculation have been transformed to form the MO integrals on disk. For large molecular systems, it may not be possible to store either set of integrals on disk, so it is desirable to formulate the matrix multiply in the atomic orbital basis. The problem reduces to finding the square matrix, F, such that the matrix multiply given in eq.(1.68) can be performed as

$$b_{ia} = \sum_{\mu\upsilon} C_{\mu i} C_{\upsilon a} F_{\mu\upsilon} \tag{1.76}$$

Consider the use of the CI-singles transition density matrix in the calculation of the contribution of the two-electron integrals to the *F* matrix:

$$F_{\mu\upsilon} = \sum_{\lambda\sigma} T^{CIS}_{\lambda\sigma}[(\mu\upsilon||\lambda\sigma)-(\mu\lambda||\upsilon\sigma)] \tag{1.77}$$

Each Davidson iteration will require one (two) of these N^2 matrices for each excited state in a spin-restricted (spin-unrestricted) calculation. They can be formed by using previously generated AO integrals or via direct recomputation of the integrals each Davidson cycle. The most efficient means of performing the AO contraction in either case is by first forming the integrals as an appropriate Raffenetti [89] combination. Subsequently, the *F* and T^{CIS} matrices can be back transformed to the MO basis:

$$F_{pq} = \sum_{\mu\upsilon} C_{\mu p} C_{\upsilon q} F_{\mu\upsilon} \tag{1.78}$$

$$T^{CIS}_{pq} = \sum_{\mu\upsilon} C_{\mu p} C_{\upsilon q} T^{CIS}_{\mu\upsilon} \tag{1.79}$$

Proving a convenient route to the intermediate arrays needed to evaluate the prefactor matrices for a CI-singles gradient calculation:

$$C1_{ci} = -2 \sum_{a} T_{ai}^{CIS} F_{ac} \quad (1.80)$$

$$C2_{bk} = -2 \sum_{i} T_{ib}^{CIS} F_{ik} \quad (1.81)$$

$$S1_{ij} = \sum_{a} T_{ai}^{CIS} F_{aj} \quad (1.82)$$

$$S2_{ab} = \sum_{i} T_{jb}^{CIS} F_{ja} \quad (1.83)$$

These expressions indicate how the energy and gradient of a CI-singles state can be evaluated without the need to store or transform two-electron integrals. A computer program has been written to perform the CI-singles gradient calculation as driven by MO integrals on disk, AO integrals on disk, or no integrals on disk. For large molecular systems where the storage of AO integrals is not possible, the "direct" calculation would provide the only means to derive excited state energies and properties in the CI-singles framework.

There are two other performance issues to mention in this section. First, a great deal of savings is realized when the prefactor matrices of eq. (1.53) are symmetrized before the matrix multiplication. Second, the diagonalization procedure is parametrized by the convergence criteria. This is the largest absolute difference between elements of the final CI-singles eigenvectors and the corresponding elements of those eigenvectors in the previous cycle. In the calculations described here, we have found that an adequate covergence criteria is 10^{-4} when only excitation energies are desired and 10^{-6} when the gradient or properties depending on the gradient are desired [89].